NSWCCD-TR-1998/026 Round Robin Damping Testing on Nonlinear Material

Naval Surface Warfare Center
Carderock Division
West Bethesda, MD 20817-5700

NSWCCD-TR-1998/026 December 1998
Carderock Division
Technical Report

Round Robin Damping Testing on Nonlinear Material

by

Edward J. Graesser and Catherine R. Wong
Naval Surface Warfare Center Carderock Division

Vikram Kinra and Danner Friend
Texas A&M University

Enrique Lavernia, Robert Perez and Jinmin Zhang
University of California, Irvine

Ahid Nashif
Roush Anatrol

Andre Riviere
Laboratoire De Mechanique Et Physique De Materiaux ENSMA

Kari Ullakko
Helsinki University of Technology

David Van Aken and Jun-Sheng Lu
University of Missouri-Rolla

Jan Van Humbeeck
NFWO MTM-K.U. Leuven

Manfred Wuttig
University of Maryland, College Park

Naval Surface Warfare Center
Carderock Division
West Bethesda, MD 20817-5700

NSWCCD-TR-1998/026 December 1998
Carderock Division
Technical Report

Round Robin Damping Testing on Nonlinear Material

by

Edward J. Graesser and Catherine R. Wong
Naval Surface Warfare Center Carderock Division

Vikram Kinra and Danner Friend
Texas A&M University

Enrique Lavernia, Robert Perez and Jinmin Zhang
University of California, Irvine

Ahid Nashif
Roush Anatrol

Andre Riviere
Laboratoire De Mechanique Et Physique De Materiaux ENSMA

Kari Ullakko
Helsinki University of Technology

David Van Aken and Jun-Sheng Lu
University of Missouri-Rolla

Jan Van Humbeeck
NFWO MTM-K.U. Leuven

Manfred Wuttig
University of Maryland, College Park

REPORT DOCUMENTATION PAGE

Form Approved
OMB No. 0704-0188

1. AGENCY USE ONLY (Leave blank)	2. REPORT DATE	3. REPORT TYPE AND DATES COVERED
	December 1998	Research and Development

4. TITLE AND SUBTITLE

Round Robin Damping Testing on Nonlinear Material

5. FUNDING NUMBERS

98-1-8420-490-10

6. AUTHOR(S)

Edward J. Graesser, Catherine R. Wong, Danner Friend, Vikram Kinra, Enrique Lavernia, Jun-Sheng Lu, Ahid Nashif, Andre Riviere, Kari Ullakko, David Van Aken, Jan Van Humbeeck, Manfred Wuttig and Jinmin Zhang

7. PERFORMING ORGANIZATION NAME(S) AND ADDRESS(ES)

Carderock Division
Naval Surface Warfare Center
Bethesda, MD 20084-5000

8. PERFORMING ORGANIZATION REPORT NUMBER

NSWCCD-TR-1998/026

9. SPONSORING/MONITORING AGENCY NAME(S) AND ADDRESS(ES)

Office of Naval Research
Arlington VA 22217

10. SPONSORING/MONITORING AGENCY REPORT NUMBER

11. SUPPLEMENTARY NOTES

12a. DISTRIBUTION/AVAILABILITY STATEMENT

Approved for public release: distribution is unlimited.

12b. DISTRIBUTION CODE

13. ABSTRACT (Maximum 200 words)

In order to assess the state of the art in damping measurements of metals, a round-robin series of damping tests was conducted. Two steels were employed in the work. One had high but nonlinear damping properties. The other was a high strength US Navy steel that had low damping properties. In this report, specimen damping test results are presented and compared. In addition, a procedure for converting from specimen damping to intrinsic damping is employed, and results are also presented on this basis. Furthermore, some test participants were able to measure the elastic modulus of the material while measuring damping, and this is also presented and discussed. It is clear from the work that large measured differences in both specimen and intrinsic damping can result when different test methods are employed. The differences are primarily attributed to systematic errors in certain testing procedures and sample design and size. In addition the method of loading and type of measurement may also account for some of the differences. A supported effort to establish a standard test sample and a standardized measurement approach is recommended to advance the state of the art in this field.

14. SUBJECT TERMS

Damping Measurements, Nonlinear Damping, Modulus, Vacrosil, HY-100

15. NUMBER OF PAGES

67

16. PRICE CODE

17. SECURITY CLASSIFICATION OF REPORT	18. SECURITY CLASSIFICATION OF THIS PAGE	19. SECURITY CLASSIFICATION OF ABSTRACT	20. LIMITATION OF ABSTRACT
Unclassified	Unclassified	Unclassified	Unclassified

CONTENTS

TABLES

FIGURES

ABSTRACT

A round-robin series of damping tests was conducted in order to clarify the state of the art in damping measurement technology as applied to metal alloys, especially those possessing nonlinear damping properties. A variety of sample designs and test procedures were employed to measure the damping capacity of a metal with nonlinear damping as well as a low damping metal. Out of nineteen volunteers who originally expressed interest in the study, ten were able to provide data from a variety of test techniques. Nonlinear damping arises when intrinsic damping in the material varies strongly with changes in the amplitude of oscillating strain. Such materials are said to have strain dependent damping characteristics. Also, for materials possessing nonlinear damping, the measured damping of a test specimen varies with strain amplitude in a manner different than the intrinsic damping inherent to a local region of material under a uniform state of strain. The importance of this distinction is addressed in this report. The two materials that were used in the work were a high damping magnetic steel (composed of iron, chromium and molybdenum), known by the tradename of Vacrosil, and a high strength steel used by the US Navy, known as HY-100 steel. The Vacrosil used in the test program possesses high intrinsic damping with strain dependent characteristics. The HY-100 steel was used as a control sample since its damping is very low and not strongly strain dependent. In this report, specimen damping test results are presented and compared. In addition, a procedure for converting from specimen damping to intrinsic damping is employed, and results are also presented on this basis. Furthermore, some test participants were able to measure the elastic modulus of the material while measuring damping. This modulus data will also be presented and discussed. It is clear from the work that large measured differences in both specimen and intrinsic damping can result when different test methods are employed. The differences are primarily attributed to systematic errors in certain testing procedures, sample design and size, but the method of loading and type of measurement may also account for some of the differences. A supported effort to establish a standard test sample and a standardized measurement approach is recommended to advance the state of the art in this field.

ADMINISTRATIVE INFORMATION

This work was conducted by the Machinery Structures Acoustics Branch, Code 842 and Materials Processing Branch, Code 612 of the Carderock Division of the Naval Surface Warfare Center (NSWCCD). This work was sponsored by the Office of Naval Research, Code 332, FRN 50015. The ONR Program Manager is Dr. Larry Kabacoff. The work was supervised by David Larrabee, Code 842 and Dr. L. Aprigliano, Code 612, Carderock Division, Naval Surface Warfare Center.

INTRODUCTION

The measurement of intrinsic damping in materials has long been used as an important tool to study microstructural characteristics in materials, such as the length of dislocation loops and the concentration of pinning sites. Intrinsic material damping measurements have also been used for nondestructive evaluation, quality control, and as an alternative approach to characterize nonmetallic and composite materials and structures [1]. Damping is also of interest as a useful feature in and of itself. For many structural/functional applications metal alloys and metal matrix composites with high intrinsic damping and modulus (HIDAMETS) offer promise for mitigation of unwanted noise and vibrations. For example, high speed turbines employ

HIDAMETS for decreased vibration and resonance suppression, and for increased fatigue life [2]. Because of the interest in high damping multiphase inorganic materials (primarily metal alloys), accurate measurements of material damping must be made for engineering, research, and design needs.

Damping tests vary in their geometry of loading and speed of oscillation. Forced steady state responses at resonance are common, as are free decay measurements and sub-resonant phase lag measurements. The types of sample deformation used in these tests are usually classified into one of the following types: longitudinal oscillation, torsion, or flexure. Test equipment varies from multi-purpose commercially available systems to those that are built "in-house" for highly specific needs. Thus, much of the data that is reported in the open literature does not follow a prescribed standard of testing. At present, there is a standard damping test (ASTM E 756), but this standard was designed for evaluation of the damping and modulus characteristics of linear polymeric materials, and not metal alloys or high stiffness composites. Furthermore, since sample types and loading vary greatly, the measured damping of a single material measured in separate devices has been shown to be very different due to the strain dependence of the material and the sensitivity of the equipment [3].

This report summarizes an effort to develop a clearer understanding of material damping as a function of strain in nonlinear high damping materials, and to develop a clear understanding of the state of the art of metal damping measurements. This understanding is necessary if advanced damping materials are to be used for reduced sound emission and structure-borne noise.

DAMPING IN ALLOYS

Damping is the dissipation of energy in vibrating systems, which results in the control of the amplitude of sustained oscillations, or their eventual decay. Many industries and military organizations employ damping technology to solve noise and vibration problems. Generally these involve addition of some form of damping treatment to vibrating structures, machines, and/or auxiliary systems. In addition to add-on damping techniques currently being used in the Navy, intrinsic material damping from highly damped alloys and metal matrix composites has been investigated as a potential means of making further advancements in the general area of damping technology and noise reduction practice. The approach has also been considered for specific component and part designs in naval seafaring and aircraft vessels that required noise mitigation.

Ideally, a high damping structural material provides a sufficient amount of both stiffness and damping so that a machine part or vibrating element can be fabricated from it without added treatments. Such materials are most useful for parts or elements subjected to mechanical oscillations that cannot be damped by conventional external (or add-on) treatments. These materials can also be useful in situations where heat or other environmental factors (e.g. moisture, erosion) have to be considered, and where add-on treatments may be expected to fail. Finally, the material approach is also useful in attenuating longitudinal vibrations that can not be damped by conventional treatments

Because high stiffness and strength are required in many important applications, metals that possess a large inherent damping capacity have been extensively sought [4,5]. Some specific applications include gears and gear webs, pump casings, engine parts, propellers, and others (see [5]). High damping metals are also used as plug inserts and cladding, and such

applications can provide a reduction of resonant amplification factors as well as the attenuation of ringing [5].

Linear Damping Properties and Low Damping Alloys

Most metals are low damping and the damping that is present is not a function of the amplitude of the vibrations. In general, the damping of metals arises from the linear anelastic behavior of the material.

Linear anelastic material behavior requires that the following conditions be imposed on stress, strain, and equilibrium in a material:

1) For each value of stress in a material there must be an equilibrium value of strain (as a corollary, this condition requires an eventual complete recovery of strain upon unloading to zero stress).

2) The equilibrium response is arrived at following some sufficient time delay (self-adjustment or relaxation).

3) A linear stress-strain relationship is required.

This definition differs from that of an ideally elastic material only in the condition imposed by item 2. For an ideally elastic material the equilibrium response is instantaneous and thus the difference between an ideally elastic material and an anelastic material is based only on the condition of instantaneous response.

The condition of linearity is assumed in derivation of the measures of damping. Many materials under low to moderate stresses (i.e. stresses much lower than the yield point) satisfy the conditions of linearity. Linearity is embodied in the principle of superposition which states that when a sequence of stresses are applied to a material at different times the newly applied stress contributes to the resulting strain as though it were acting alone. In more specific terms this means that if there exists a stress history $\sigma_1(t)$ which produces a strain history $\varepsilon_1(t)$, and a separate stress history $\sigma_2(t)$ which produces a strain history of $\varepsilon_2(t)$, then the sum $\sigma_1(t) + \sigma_2(t)$ will produce a strain of $\varepsilon_1(t) + \varepsilon_2(t)$.

One measure of damping is known as the loss factor, η. The loss factor of a typical machinery system is on the order of 10^{-2} to 10^{-1}. Most structural metals like HY-100 have a loss factor on the order of 10^{-4} therefore the effect of the damping capacity of the material on the damping capacity of the system is negligible.

Amplitude Dependence and High Damping Alloys

Generally the loss factor of a "high damping" metal is on the order of 10^{-2} or higher. Indeed many alloy compositions have been studied and found to possess such levels of damping (e.g. see [2 – 9]). Mechanisms that give rise to damping in metals include the movement of point defects, dislocations, and domain walls. These effects give rise to macroscopic hysteresis in the stress strain curve and thus damping. Such processes may be frequency independent and occur well below the threshold for plastic deformation. The damping capacity of high damping metals is strain dependent (i.e. nonlinear) because the primary damping mechanisms function over a finite strain range. That is, a minimum stress is required to move the microstructural element, and when the element has moved through its full range, additional stress will not move it further. Such effects often give rise to a well-defined peak in the plot of measured damping vs. specimen strain amplitude.

Strain dependent response is termed "nonlinear" because the measured damping capacity varies with specimen strain amplitude. A generalized stress-strain diagram corresponding to a relatively large category of nonlinear damping mechanisms is illustrated in Figure 1. At low stresses (below σ_t) and strains, damping is generally low. As the amplitude of cyclic stress is increased a threshold stress, σ_t, is reached. At amplitudes above this threshold, a damping mechanism is activated, causing hysteresis. However, as the amplitude of cyclic stress (or strain) is increased further, the mechanism becomes saturated . A characteristic saturation strain is used to designate this phenomenon, typically denoted as ε_0. There is no appreciable hysteresis above ε_0.

This type of hysteretic response can be associated with a number of nonlinear anelastic damping mechanisms. For example, in dislocation breakaway a minimum stress is required to force dislocations over nearby pinning points during loading. Upon unloading, the elastic strain energy stored in the lattice of the material may be sufficient to move the dislocations back to their original positions. The net effect of this process is in essence an elastic response with damping.

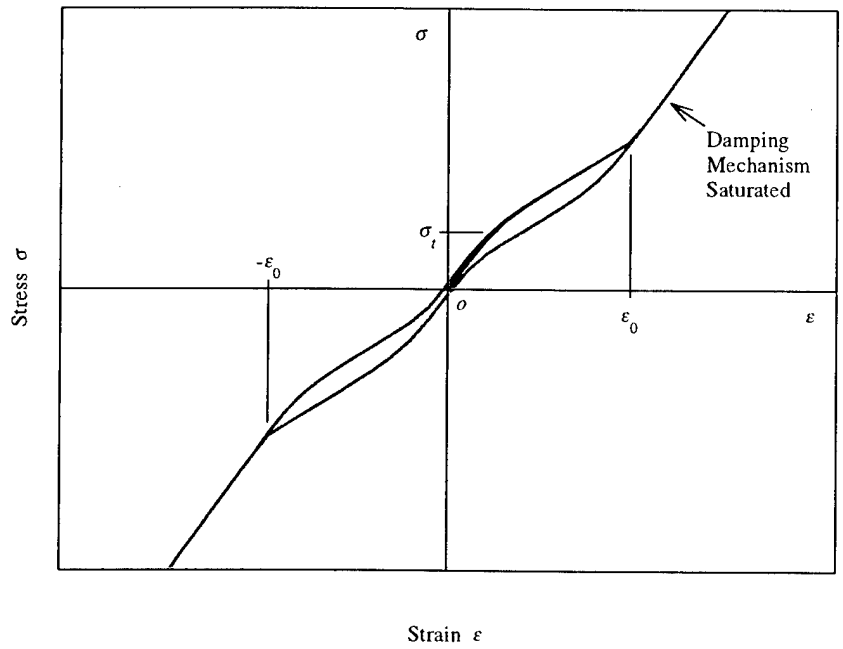

Figure 1. Generalized stress-strain hysteresis for material possessing strain dependent damping.

The measure of damping that will be used for presentation of results in this report is loss factor, denoted by the symbol η. The loss factor is defined as

$$\eta = \frac{\Delta W}{2\pi W} \tag{1}$$

where ΔW is the energy dissipated every cycle, as illustrated in Figure 2, and W is the strain energy in each cycle, as illustrated in Figure 3.

Other nonlinear anelastic damping mechanisms include the movement of mobile domain boundaries. Ferromagnetic domain walls, twin boundaries, antiferromagnetic domain walls, and phase domain walls fall into this category. A finite amount of stress (σ_t) is required to initiate this type of mechanism, i.e. a specific amount of stress is required to overcome an energy barrier so that the boundaries may move. Subsequently, the boundaries reorient to the applied stress, causing dissipation. Release of the applied stress subsequently causes the mechanism to act in reverse because the elastic strain energy stored in the material is sufficient to move the boundaries back across the energy barrier. The net effect is an elastic response with energy dissipation due to internal friction. It is again emphasized that these mechanisms become saturated at a limiting value of strain.

For example, the magnetic domains in high damping ferromagnetic alloys are arranged in a randomly oriented pattern when the material is unstressed. Upon application of cyclic stress or strain, the domains change their orientation and tend to align themselves in the direction of loading as the load level is increased. Internal friction derives from the interaction of domain boundaries, thus causing dissipation. Below ε_0, the intrinsic damping increases with increasing strain; this is the region where the damping mechanism is active, and the level of dissipation increases with increasing strain amplitude. However, once the domains become fully aligned (at strains above ε_0) further loading cannot cause relative motion of the domains and the mechanism is said to be saturated. Above the saturation point, the level of dissipation (ΔW) becomes constant, but the stored energy W continues to rise. Therefore, for strain levels in excess of ε_0, the amount of energy that can be dissipated by this type of mechanism is limited to a fixed value, and the loss factor decreases with increasing amplitude of loading. These features are shown for a family of high damping ferromagnetics in Figure 4. The peaks shown in this figure are indicative of the saturation strain ε_0.

The data obtained for a single strain dependent material in varied test configurations are often difficult to compare because of the inherent strain distributions that arise from the loading. All tests which are used for characterization of damping apply loading to a sample in such a way that strain distribution in the sample is non-homogeneous. When testing a sample of material possessing nonlinear damping, the experimentalist must record damping as a function of strain (or stress) amplitude. However, since strain is non-homogeneous in the sample volume, different values of damping will arise in different tests.

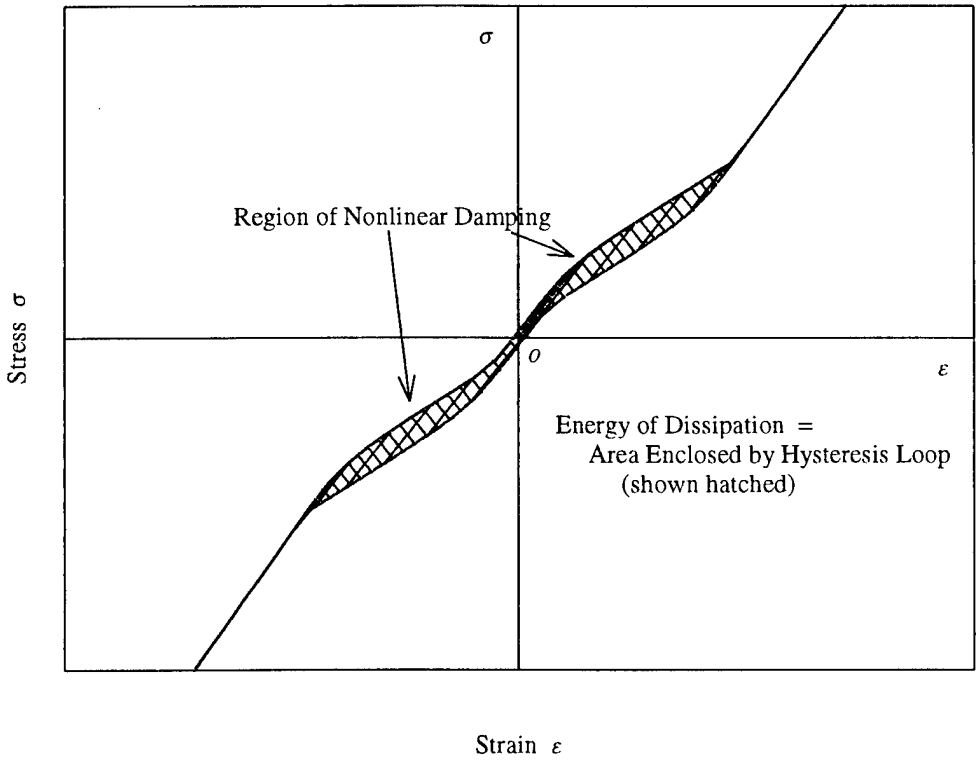

Figure 2. Hysteretic dissipation energy for material with nonlinear damping.

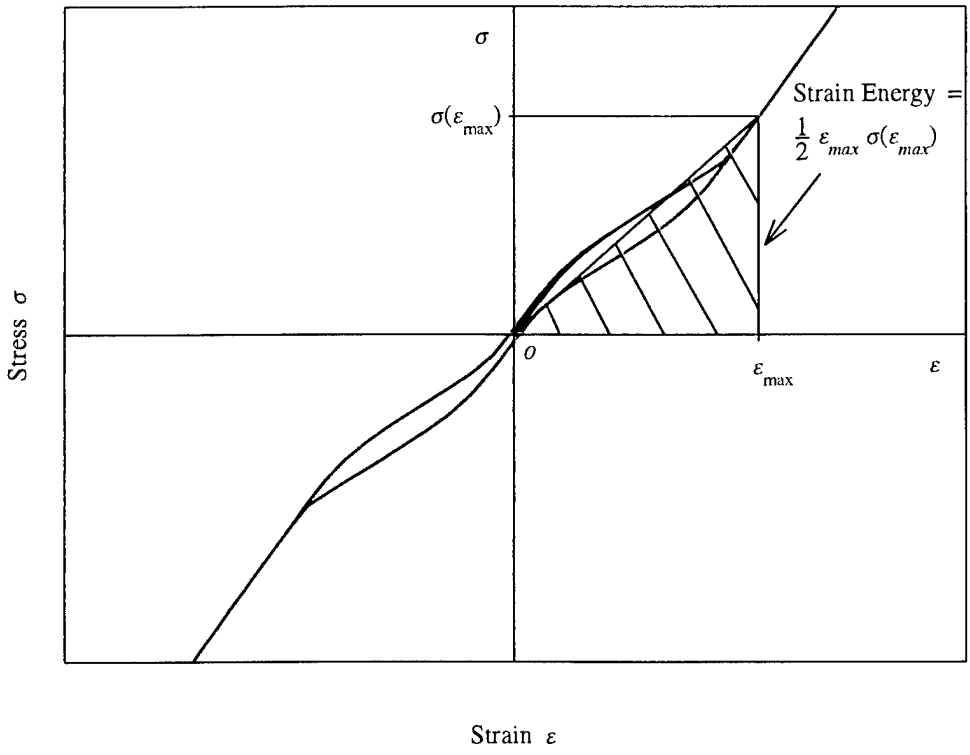

Figure 3. Measure of strain energy for material with nonlinear damping

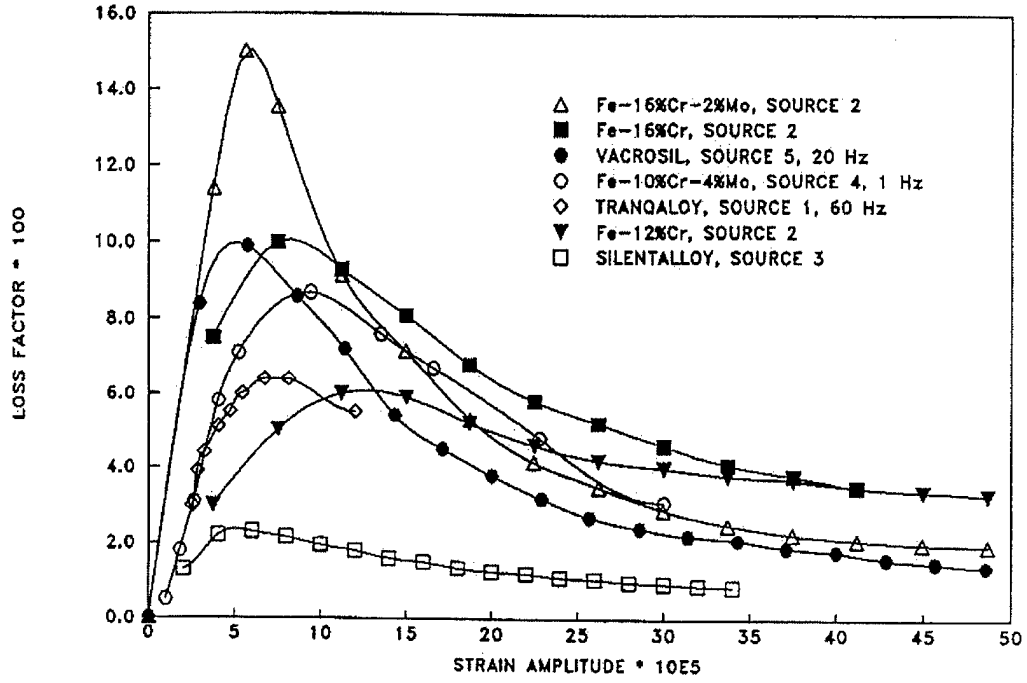

(1) Nippon Kokan K.K., Tranqaloy Data Sheets, 1981

(2) K. Suzuki et. al, Internal Friction and Ultrasonic Attenuation in Solids, pp757, 1977

(3) H. Kawabe and K. Kuwahara, Trans. Jap. Inst. Metals, Vol. 22, No. 5, pp301, 1981

(4) H. Masumoto, 1984

(5) W. Schneider et.al., J. De Physique, Vol. 42, No. 10, ppc5-635, 1981

Figure 4. Loss factors for variations of the Fe-Cr alloys measured by a variety of methods.

Data from separate bending and torsion tests [3] show this effect; indeed the results indicate that the torsional tests produce significantly higher values of damping at the same levels of peak sample strain as shown in Figure 5. Also, the damping rises more steeply with peak sample strain in the torsion test. However, it is important to note that the strains on the abscissa are shear strains in the case of torsional data and axial strains in the case of bending data. These separate strains are not equivalent; indeed axial strains give a measure of length change while shear strains refer to the distortion of right angles.

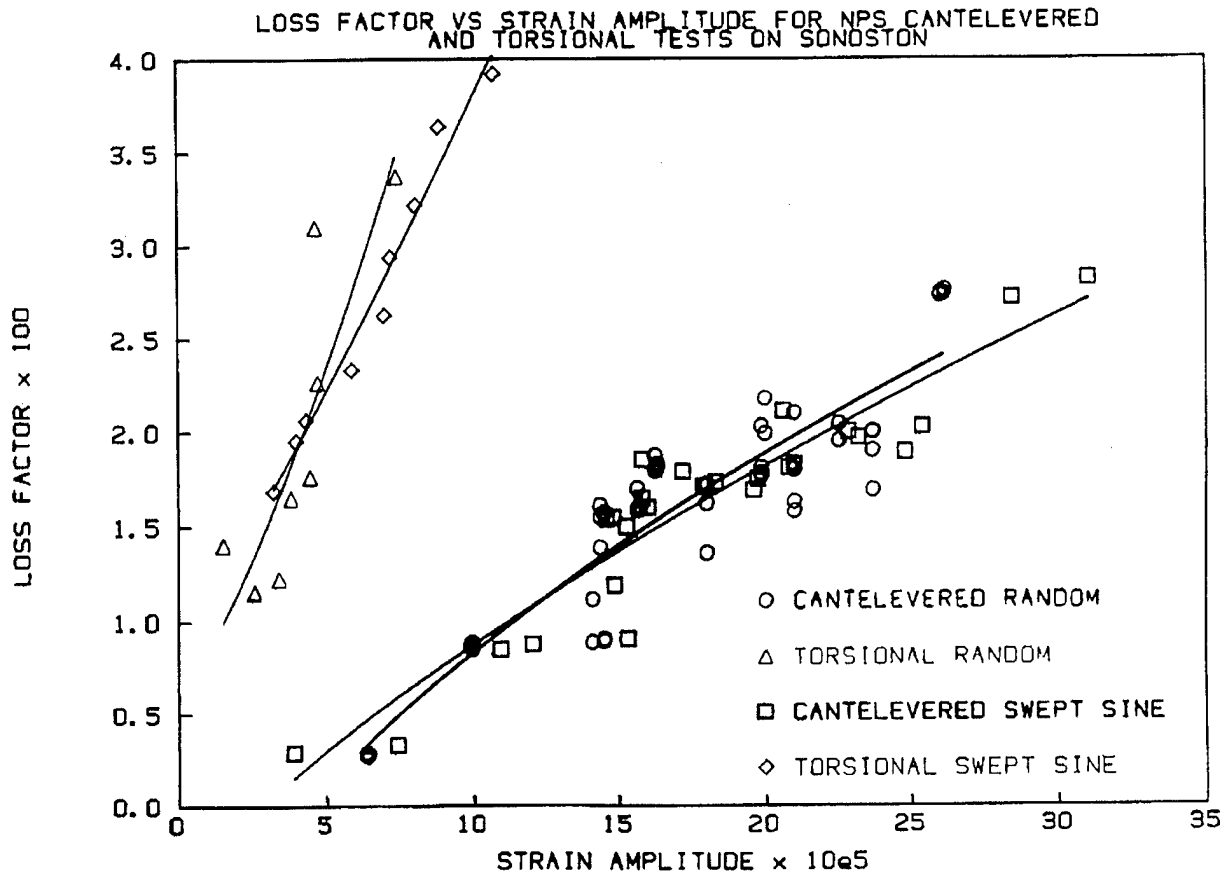

Figure 5. Loss factor for non-linear metal test by different methods.

Ultimately, a standard procedure is needed to address these inconsistencies. Such a procedure will necessarily involve deconvolution of measured specimen damping (from tests on whole samples), to intrinsic damping of the material. Important references on this topic include [10 - 13]. The intrinsic damping is that which would arise if the sample were stressed/strained uniformly (or homogeneously). To this extent, Roatta et. al [13] have shown that deconvolution to intrinsic strain is important for consistent damping results arising from separate torsion tests on cylinders and parallelepipeds. Also, Graesser and Wong [14], have proposed a correlation method which is intended to produce consistent results when considering separate axial, bending, and torsion tests.

A round-robin program was started in response to these issues. However, it is not intended to solve all these problems and to set forth a proposed standard in this report. Instead, the emphasis was placed on the study of results from tests of round-robin samples, and the comparison of data on a measured basis, as well as on an intrinsic basis. To do this, a high damping ferromagnetic material with nonlinear damping (Vacrosil) was used as a test material. A low damping Navy steel, HY-100, possessing linear damping and known modulus was used as a control material.

Magnetic alloys, like Vacrosil, which have large magnetostriction often have a high damping capacity. Magnetostriction is the tendency of magnetic domains to line up parallel to

the direction of applied tensile stress. Generally these materials have peak damping at strain amplitudes between 10^{-5} to 10^{-6}. Other commercial alloys that have been specifically developed to exploit this type of damping include the Co based alloy Nivco 10, and the Fe based alloys known as Silentalloy and Gentalloy.

Cochardt, [15] as well as Smith and Birchak [16] proposed methods of calculating the intrinsic material damping based on the mechanism of movement of magnetic domain walls. Others [10-13] have pointed out the need for a method for calculating the intrinsic material damping from specimens subjected to inhomogeneous applied stress in the amplitude dependent range based on the stress distribution in the sample. A relationship is derived in [10] for measured specimen loss factor (η_s) as a function of maximum sample strain, in terms of strain distribution in the sample volume ($dV/d\varepsilon$) and local (or intrinsic) material loss factor (η) as follows:

$$\eta_s(\varepsilon_{\max}) = \frac{\int_0^{\varepsilon_{\max}} \eta(\varepsilon)\varepsilon^2 \frac{dV}{d\varepsilon} d\varepsilon}{\int_0^{\varepsilon_{\max}} \varepsilon^2 \frac{dV}{d\varepsilon} d\varepsilon} \tag{2}$$

The above equation can be used for either of two purposes: (1) substituting theoretical expressions for $\eta(\varepsilon)$ and $dV/d\varepsilon$ and comparing computed curves for η_s to measured data, or (2) converting measured values of $\eta_s(\varepsilon_{max})$ to $\eta(\varepsilon)$ after correcting for inhomogeneous stress. In the second case, the resulting $\eta(\varepsilon)$ could be compared to theoretical models, (e.g. see Ritchie and Pan [17]), or to other sets of intrinsic damping data. Equation (2) above can be solved for intrinsic damping when special conditions of loading are specified. A summary of equations for conversion of measured internal friction to intrinsic internal friction at constant maximum strain amplitude is found for torsion, longitudinal vibration, and flexure in [12]. These are repeated in the following section.

Please note that the relationships are valid for sub-harmonic oscillations and n=1 modal conditions (i.e. first mode resonance). Conversion to intrinsic damping at higher order modes requires use of different formulae not reported here.

DAMPING MEASUREMENT CONCEPTS

There are several ways to measure damping and the techniques can be grouped by the method of oscillation used in a given measurement. Every technique has a unique method of holding the sample, introducing the vibration into the sample and measuring the sample's response. All methods require samples with a specific geometry that varies with the method as well as the apparatus. Because of this the strains introduced into the samples will vary. Relationships for determination of intrinsic damping based on common specimen shapes and loading conditions are delineated in the following sections.

Longitudinal Oscillations in a Bar

The method is applied to rods of material with either square or circular cross-section. This method of testing was first invented by Marx [18] for sustained oscillations at resonance, using a composite oscillator. As the method became widely used it was subsequently referred to as PUCOT (Piezoelectric Ultrasonic Composite Oscillation Test).

The formula that relates specimen damping to intrinsic damping for longitudinal oscillation is as follows [10]:

$$\eta(\varepsilon) = \frac{1}{2\sqrt{\varepsilon}} \frac{d}{d\varepsilon} \left\{ \int_0^{\varepsilon} \frac{\eta_s(\varepsilon_0)\varepsilon_0}{\sqrt{\varepsilon - \varepsilon_0}} d\varepsilon_0 \right\} \tag{3}$$

where ε represents axial strain, ε_0 represents the maximum strain in the sample, η_s is the specimen damping and η is the intrinsic damping. Damping is first measured using a specimen of known geometry, under known conditions of strain. Specimen damping is then recorded as a function of the amplitude of the maximum strain in the sample. The specimen damping data is then curve-fit using an analytical formula, with the result denoted as $\eta_s(\varepsilon_0)$. The analytical formula for specimen damping, $\eta_s(\varepsilon_0)$, is then substituted into the above equation, followed by appropriate algebra and calculus. This yields the intrinsic damping as a function of strain: $\eta(\varepsilon)$. The case of a polynomial curve fit to specimen damping, and conversion to intrinsic damping is given in Appendix A.

Torsion Loading

Tests are done in torsion at both sub-harmonic and resonant conditions. Strain dependent damping is designated as a function of shear angle: $\eta(\gamma)$. The relationship between intrinsic damping and specimen damping, η_s, is as follows for samples of circular cross-section [10]:

$$\eta(\gamma_s) = \eta_s(\gamma_s) + \frac{\gamma_s}{4} \frac{d\eta_s(\gamma_s)}{d\gamma_s} \tag{4}$$

where γ_s represents the value of the shear angle (which is twice the engineering shear strain) on the outer surface of the sample. The sample's cross section in this case was rectangular and so there is some error is made using this relationship for a circular cross section. However, the error is small. This process again involves curve-fitting of measured data, producing an analytical form for $\eta_s(\gamma_s)$. The intrinsic damping is then computed with the above equation.

Cantilever Beam

Damping tests are common on cantilever beams. These are beams that are fully clamped at one end and free at the other. Loading is applied to the free tip. Sustained resonance and free decay are conventional conditions from which damping is measured. The formula for computing intrinsic damping as a function of axial strain due to bending is as follows [11]:

$$\eta(\varepsilon_s) = \eta_s(\varepsilon_s) + \frac{7}{9}\varepsilon_s \frac{d\eta_s(\varepsilon_s)}{d\varepsilon_s} + \frac{1}{9}\varepsilon_s^2 \frac{d^2\eta_s(\varepsilon_s)}{d\varepsilon_s^2} \tag{5}$$

where ε_s is the amplitude of strain on the surface of the beam at the root of the cantilever; η_s is the measured damping of the specimen, and η is the intrinsic damping. The procedure for measurement and deconvolution is analogous to that for torsion, as discussed previously; only the form the of equation is different. A derivation of this formula is given in Appendix B.

Fixed Guided Beam

These tests are done on beam samples that are clamped on both ends. One end is held fixed and the other end is deflected while continuing to be held in stiff clamps. Commercial

apparatus that use this approach include Rheometric Scientific DMTA (Dynamic Mechanical Thermal Analyzer) and the Dupont Corporation DMA (Dynamic Mechanical Analyzer). The form of the conversion equation is identical to that of the cantilever beam. A derivation is given in Appendix B.

$$\eta(\varepsilon_s) = \eta_s(\varepsilon_s) + \frac{7}{9}\varepsilon_s \frac{d\eta_s(\varepsilon_s)}{d\varepsilon_s} + \frac{1}{9}\varepsilon_s^2 \frac{d^2\eta_s(\varepsilon_s)}{d\varepsilon_s^2} \tag{6}$$

where ε_s is the amplitude of strain at the surface of the beam; η_s is the measured damping of the specimen, and η is the intrinsic damping. A derivation of this formula is given in Appendix C.

MEASUREMENT METHODS TO OBTAIN SPECIMEN DAMPING

The following sections describe different test methods used to obtain the damping of a specimen of material.

Free Decay of Oscillations

This damping test first involves steady state excitation of a cantilever or torsion specimen, generally at first mode resonance. The excitation source is then switched off, and the oscillations are allowed to decay freely. The free decay of vibration amplitude is recorded. This is illustrated in Figure 6. Since the specimen vibrates at a resonant frequency the geometry of the sample must be changed to be able to test at different frequencies. Or, one must preferentially excite higher order modes and measure their decay (however, this adds complexity for assessment of intrinsic damping, and one must be certain that the selected mode of vibration does not convert to a different mode as free decay progresses). The number of cycles over which the damping is measured is a function of the damping capacity of the sample, with low damping materials measured over many cycles and high damping samples measured for only a few cycles.

It should be noted that measurements of free decay on amplitude dependent samples could lead to difficulties in accurate determination of intrinsic damping. This was pointed out by Povolo [19] and by Ritchie et. al [20]. Average log decrement values are usually measured over a range of n amplitudes. If n is large then the average value can be grossly different than the true value if amplitude dependence is strong. However by appropriate numerical techniques [19, 20] the average value of free decay damping can be made to be a good estimate of the actual amplitude dependent damping.

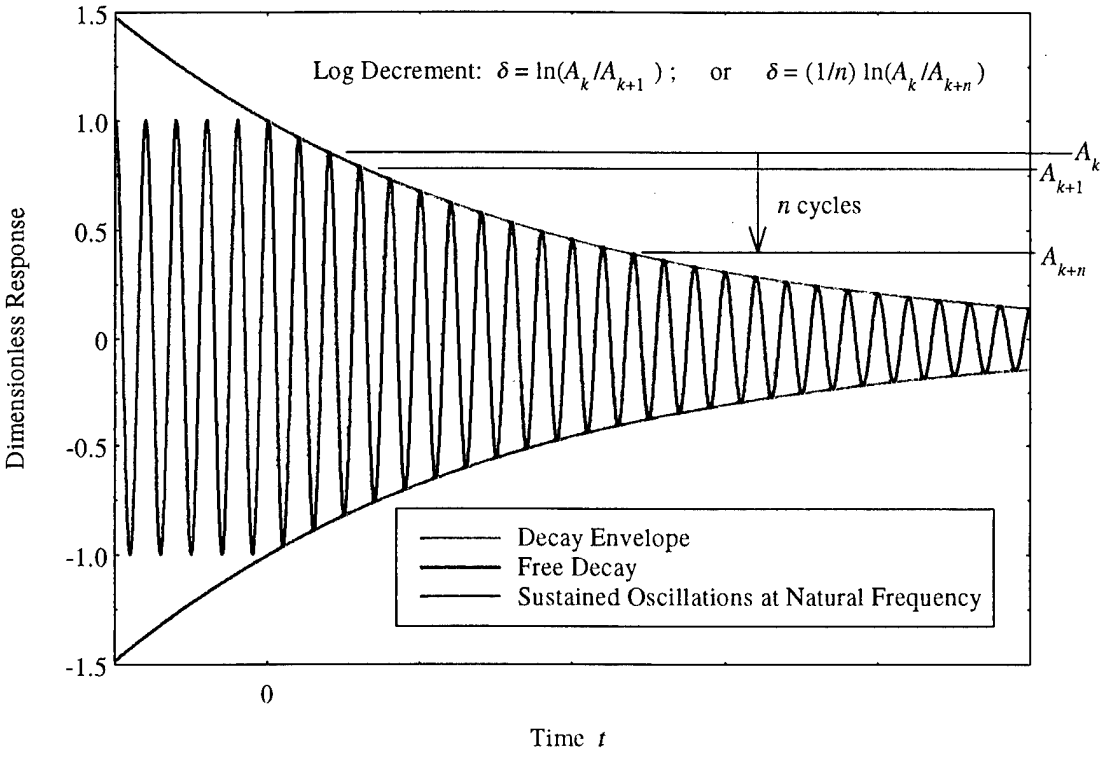

Figure 6. Graphic representation of logarithmic decrement.

For linear materials the free decay of a cantilevered beam is

$$y(t) = A_0 e^{\frac{-\Psi\omega t}{4\pi}} \cos(\omega t + \alpha)$$

where $y(t)$ is the vibration (displacement, velocity, or acceleration) at time t, A_0 is the amplitude during the first cycle, ω is the circular frequency, α is phase and Ψ is the specific damping capacity [21]. Measuring A_n, the amplitude of vibration of the nth peak, plotting $\ln(A_0/A_n)$ versus the peak number and fitting a straight line passing through the origin, leads to the specific damping capacity Ψ

$$\Psi = 2m \tag{7}$$

where m is the slope of the line.

Alternatively the log decrement, δ, can be directly used as a measure of damping. δ is defined as either of the following:

$$\delta = \ln(A_n/A_{n+1}) \qquad \text{[for one cycle]} \tag{8}$$

$$\delta = \frac{1}{n}\ln\left(\frac{A_k}{A_{k+n}}\right) \qquad \text{[for a small number of cycles, } n\text{]} \tag{9}$$

where A_n and A_{n+1} are vibration amplitudes for successive cycles of free decay in the first equation, and A_k and A_{k+n} are vibration amplitudes at the beginning and end of n successive cycles of free decay in the second equation.

To measure the damping capacity of nonlinear material, the decay profile can be divided into blocks of several cycles. If the block contains a sufficiently small number of cycles, the decay in strain amplitude is small and so the change in Ψ is small. Therefore the damping is assumed to be constant within each block and the theoretical model adequately describes the experiment. The measured damping within the block is assigned to the stain amplitude at the mid-point of the block.

Forced Resonance

This damping measurement method involves either transverse vibration of a cantilevered beam or axial twisting of a bar, at resonant frequency. The technique is to measure the bandwidth of the resonance peak at half maximum (referred to as 'half-power bandwidth') and the natural frequency associated with resonance; this is shown in Figure 7. An equivalent approach for measuring the half-power bandwidth is to determine the frequency separation 3.0 dB below the resonance peak (which gives rise to the name '3 dB down method'); this is shown in Figure 8. Again, the sample size must be changed in order to change the test frequency. Or, more commonly, multiple modes must be recorded and analyzed for half-power bandwidth and natural frequency. The half power bandwidth and 3 dB down tests produce the same result (they are in fact the same test), and lead directly to the measure of damping called inverse quality factor, Q^{-1} :

$$Q^{-1} = \frac{\Delta\omega}{\omega_n} = \frac{\omega_2 - \omega_1}{\omega_n} \tag{10}$$

where ω_n is the natural frequency and $\Delta\omega$ is the half-power bandwidth. The frequencies ω_2 and ω_1 are the half-power frequencies where, by convention, $\omega_2 > \omega_1$.

It should be noted that accurate determination of the resonant frequency is necessary for a reliable measurement of damping. Automatic resolution features offered on modern analyzers, combined with zoom analysis (fine resolution), allow for a reasonably accurate measurement of the natural frequency. However, one should check that the resonance frequency is truly accurate by use of circle-fit procedures, as described in Ewins [22]. A number of modern modal analysis software packages directly employ circle-fit methods for natural frequency determination.

To determine amplitude dependence via inverse quality factor measurements, the sample must be excited to known vibration amplitude levels, and one must be able to convert from vibration amplitude to strain (requiring knowledge of deflection amplitudes and mode). One must be able to do so on a repeatable and reliable basis. It must also be possible to vary the vibration amplitude over a reasonable range.

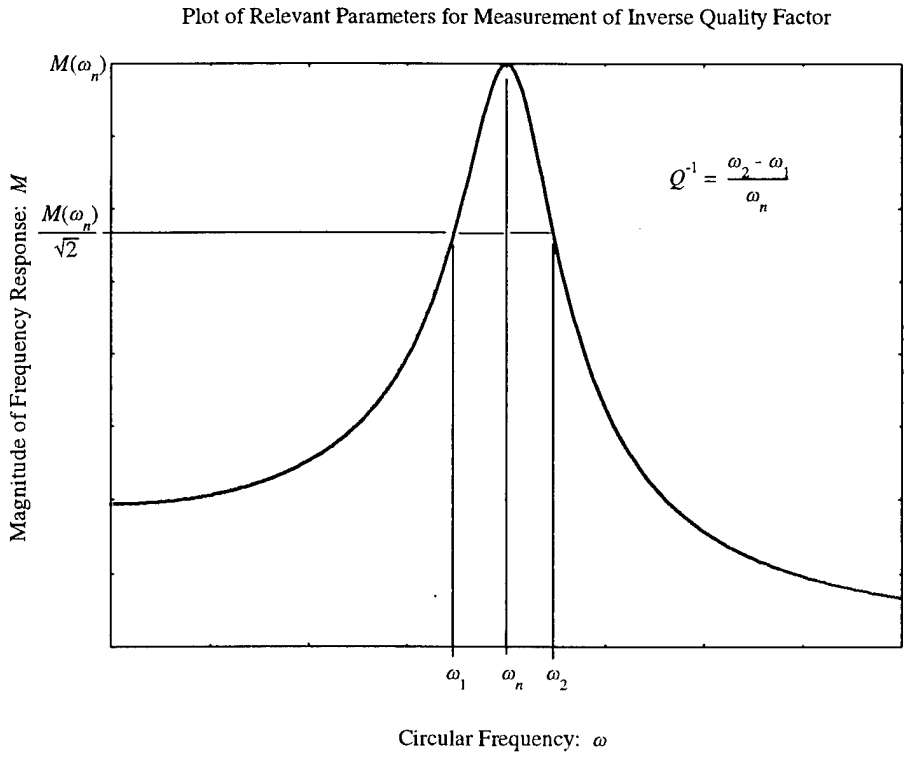

Figure 7. Plot of relevant parameters for measurement of inverse quality factor.

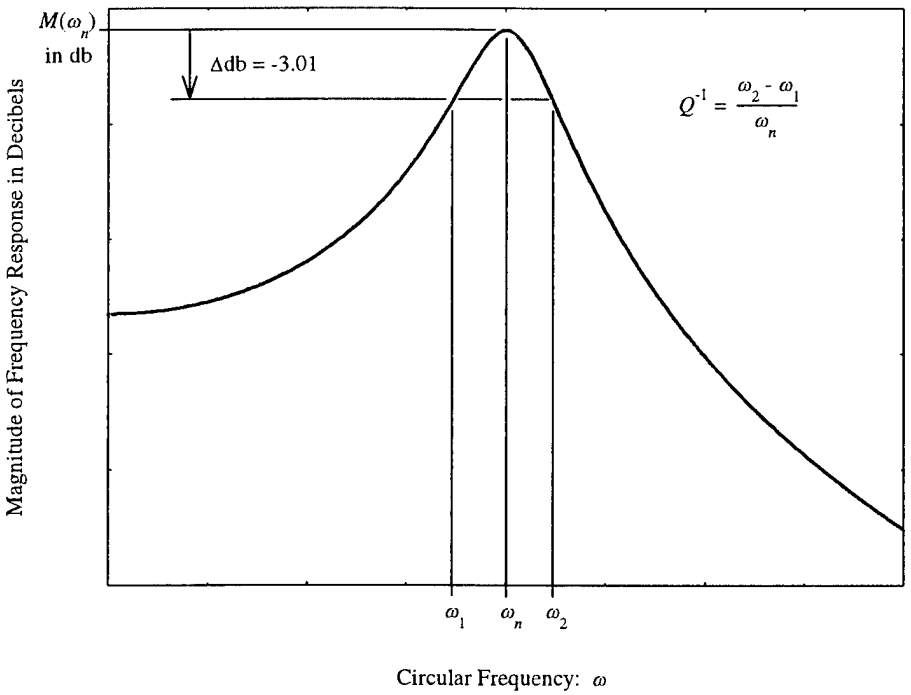

Figure 8. Inverse quality factor according to the "3 dB down" method.

Deconvolution to intrinsic damping, by the equations presented earlier, is possible only for excitation of the first mode of vibration (and no others). The deconvolution equation is not valid for higher order modal oscillations or broadband vibrations. New equations need to be derived for tests which involve preferential excitation of higher order modes (i.e. excitation of individual modes, such as second mode, third mode, etc.). Also, a process would need to be developed for deconvolution under random and/or chirp broadband excitations.

It can be shown [23] that for cases where damping levels are not in excess of $Q^{-1} = 0.14$, the measures Q^{-1} and η are nearly identical. For this reason, Q^{-1} and η are often used interchangeably.

Sub-Harmonic Oscillation (Phase Lag and Loss Factor)

This method of measuring involves applying a small sinusoidal time-varying mechanical force and measuring the displacement of the sample. The phase angle, ϕ, of the lag between the applied load and the measured displacement is recorded. The tangent of ϕ is a measure of the damping capacity. For simple linear models tan ϕ is exactly equal to η [23], and for this reason it is often called the loss factor.

Comparison of Damping Measures

All the measures of damping capacity described above are unitless and assume that the materials are homogeneous and linear. The most common measures are loss factor and specific damping capacity. They can be interrelated by their inherent definitions [23] when damping levels are within the range $0 < \eta < 0.14$.

$$\eta = \psi/2\pi = \delta/\pi = Q^{-1} = \tan \phi \qquad (11)$$

MATERIALS AND TEST SAMPLES

METAL ALLOYS

The two alloys used in this study were Vacrosil and HY-100 steel (MIL-S-16216). The chemical composition of these alloys are given in Table 1. All the Vacrosil samples were taken from the same casting which was produced by Vacuumschmeltze GBD, and then vacuum arc re-melted a second time. All the HY-100 samples were taken from the same plate, produced by USX.

TEST SAMPLE DESIGNS

Since each test method required a specific sample size, it was not possible to make one sample to be tested on all apparatus. Therefore, a sample was made for each method as shown in Figure 5. The correlation between samples and test methods is listed in Table 2.

Table 1. Composition of Vacrosil and HY-100 in weight percent.

Element	Vacrosil (wt%)	HY-100 (wt%)
Fe	83.5	remainder
C	0.003	0.155-0.165
Cr	12.5	1.66-1.69
Mo	2.36	0.57-0.59
Mn	0.29	0.36-0.37
P	0.008	0.013-0.014
S	0.005	0.005
Si	0.17	0.23-0.25
Cu	0.79	0.14
Ni	0.037	3.22-3.26
Sn	--	0.005-0.008
Al	0.037	0.17-0.27
V	0.005	0.008-0.009
Ti	0.005	0.003
N	0.006	--
O	0.011	--

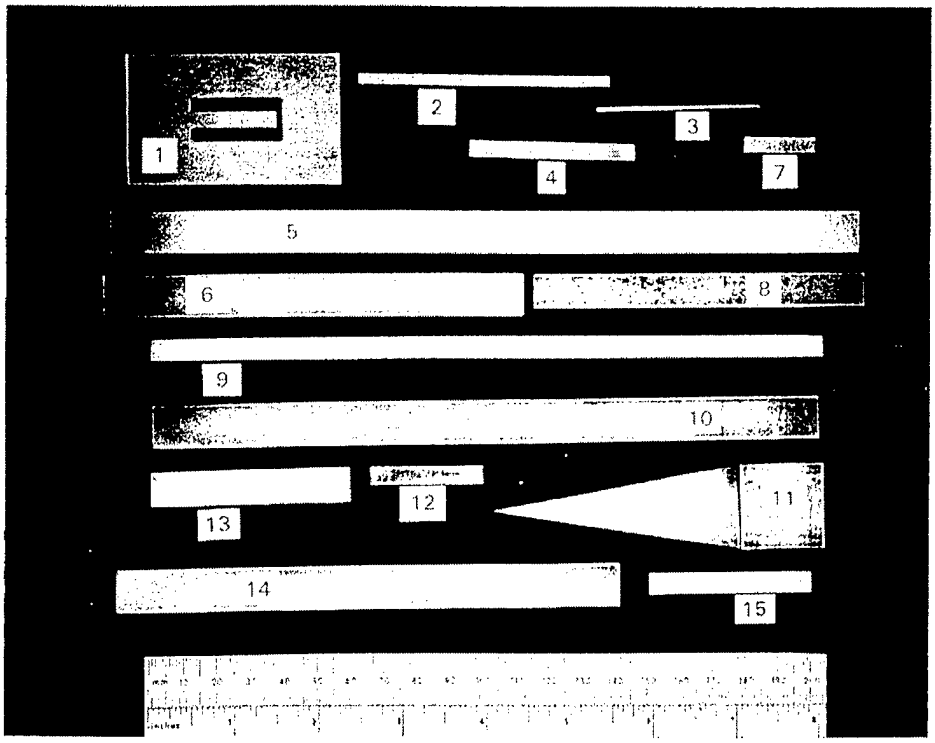

Figure 9. Samples made for test methods.

Table 2. Method/Sample correlation with Figure 5.

Method	Sample	Sample dimensions (in)		
		thickness	width	length
A	10	0.125	0.5	8.0
B	1	0.027	0.19	1.0
C	Not pictured	0.038	0.04	2.0
D	11	0.038	1.0*	3.0
E	13	0.60	0.20	2.0
F	2	0.124	0.123	2.4
G	3	0.06	0.06	1.9
H	15	0.06	0.40	2.4
I	12	0.039	0.20	1.4
J	8	0.06	0.40	4.0

*measured at root.

FABRICATION OF TEST SAMPLES

Blocks of material were cut from the casting or plate. The HY-100 was used in the quenched and tempered state. Oversize bars of Vacrosil were heat-treated before final specimen preparation. The heat treatment was performed in order to remove internal residual stress and optimize intrinsic damping. The heat treatment used was the same as that specified in Schneider et. al [6]. The heat treatment consisted of 1100°C for one hour and slow cooling in an argon filled chamber. The argon was maintained during the entire heating and cooling process. Cooling took place gradually, over nine hours.

All Vacrosil samples were fabricated from these blocks using wire electrical discharge machining (EDM) as shown in Figure 10. The EDM method minimizes the possibility of residual stress, which would otherwise occur in sawing, milling, and grinding steps. Residual stress would affect the damping of the specimen, leading to an erroneous measure of the property. Magnetic fixtures were also avoided. Sustained magnetic fields (such as those generated by surface grinding machines) could have caused a permanent change in the magnetic domain structure of the material samples, which could bias the damping data. Samples were taken from the interior of oversize bars. A flat surface was cut on one face and then slices were taken to make parallel faces of precise thickness. Individual samples were then cut to size from the slice, again using EDM.

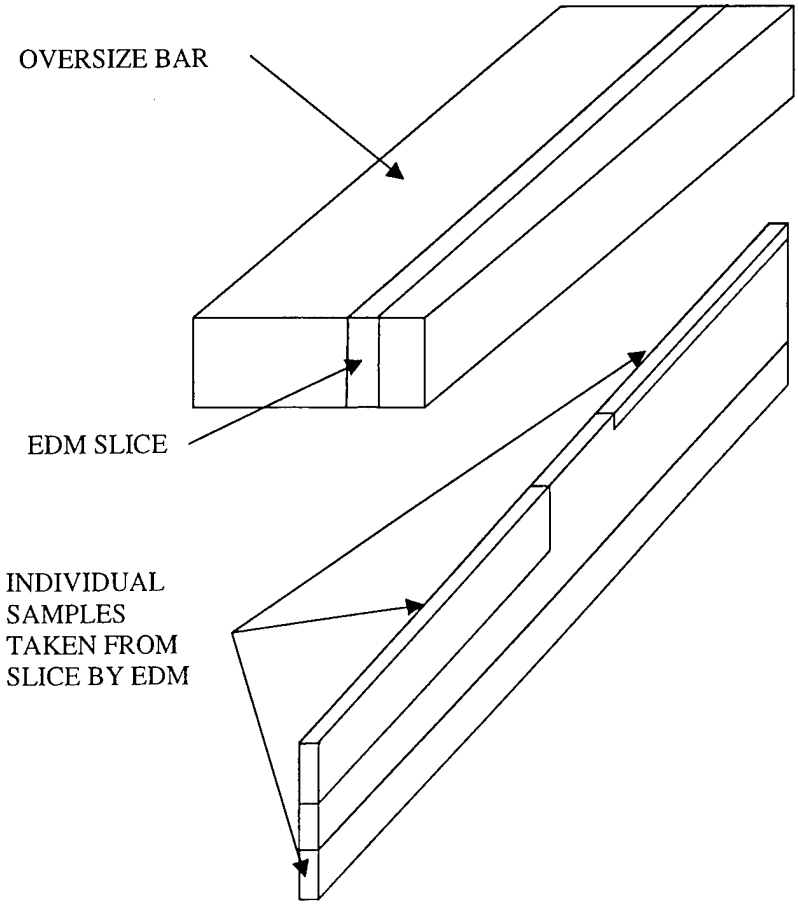

Figure 10. System of sample fabrication.

MICROSTRUCTURE OF VACROSIL

In order to examine the microstructure of the Vacrosil, samples of the material were polished and etched. The large grains and subgrains of the as-cast microstructure are shown in Figure 11. After heat treating the microstructure was essentially unchanged as shown in Figure 12. Both microstructures also contain undissolved inclusions. Energy dispersive spectroscopy was performed on a Noran Voyager EDS system and the results are presented in Figure 13. The inclusions may be MnS or Al_2O_3. Si and Mo are also present.

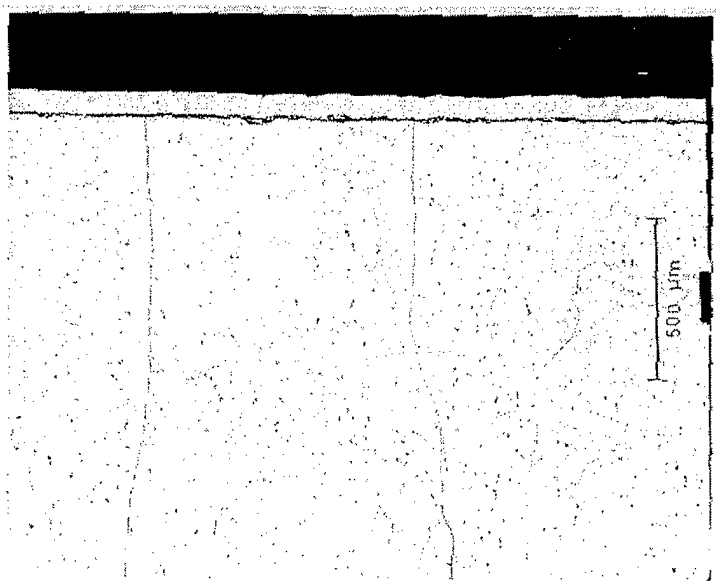

Figure 11. Microstructure of as-cast Vacrosil near the cast edge. (Vilella's etch)

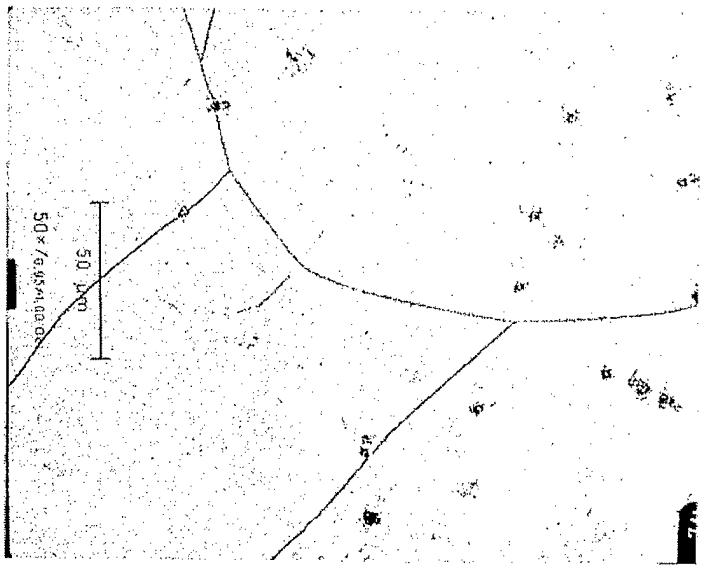

Figure 12. Microstructure of heat treated Vacrosil. (Vilella's etch)

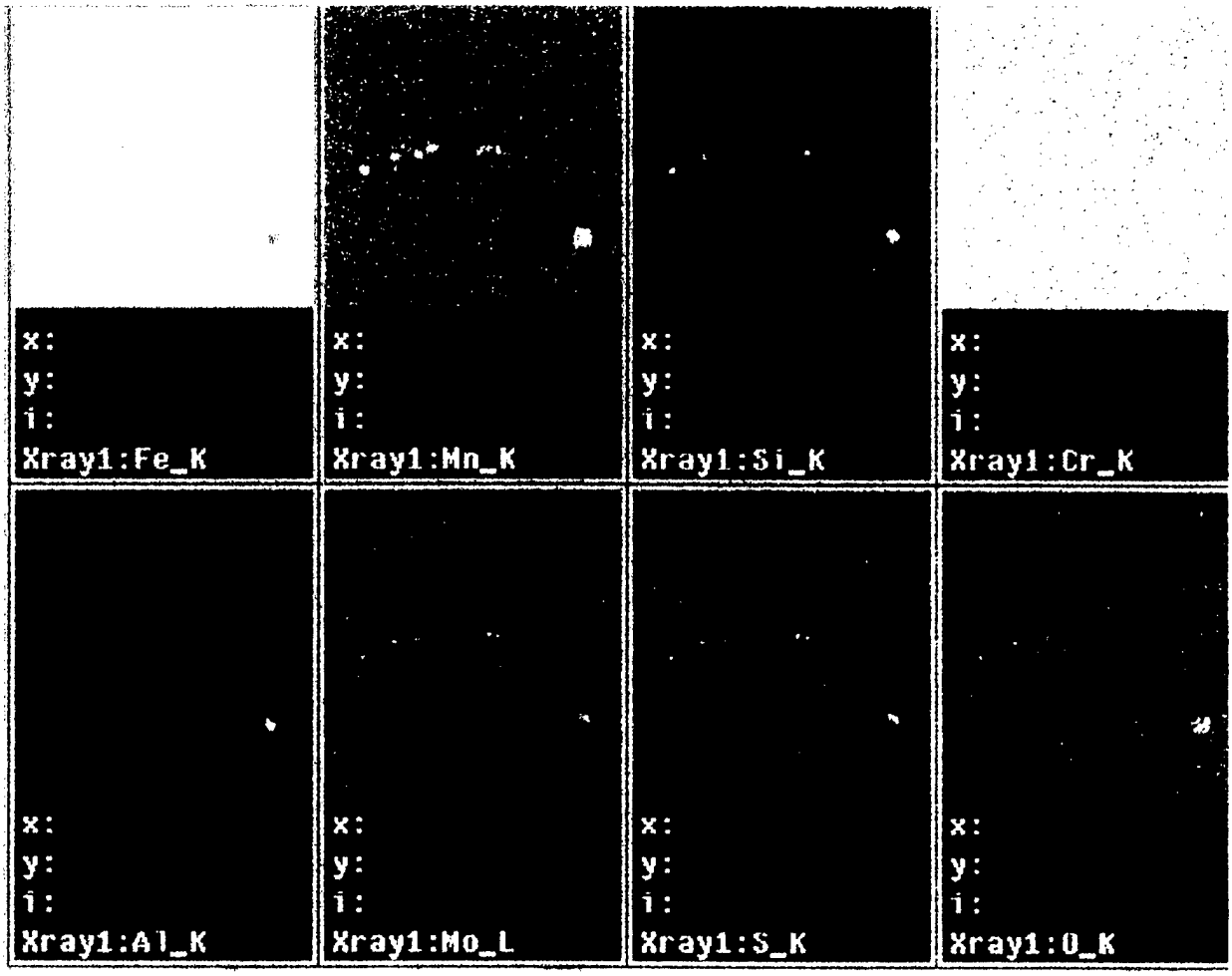

Figure 13. Elemental maps of Vacrosil inclusions.

On some samples, EDM made unexplained parallel lines on the surface of the metal as shown in Figure 14 and Figure 15. These marks penetrated a short way into the surface as shown in Figure 16. In cases where the samples were small in thickness, the samples were polished to remove these marks when possible. In other cases samples were re-made in an attempt to procure a new sample without the surface anomalies. Invariably, some lines were seen on most samples. However, samples that were sent out for testing had only a few of the anomalies, or the lines were removed by metallographic polishing.

Inquiries on this question were made with the manufacturer of the EDM (Hitachi) unit, but no-one could explain the nature of the observed lines. It is possible that, during spark melting, local regions of metal with high concentrations of Cr were melted to a slightly greater depth, forming the observed surfaces. Or there could have been an interaction of the EDM arc with selected magnetic domains at the surface of the Vacrosil, causing slightly more aggressive melting in those select regions, and the observed lines.

Despite these minor difficulties, the fabrication process that was used produced the best possible samples with uniform properties and no residual stresses nor exposure to strong magnets or magnetic fields.

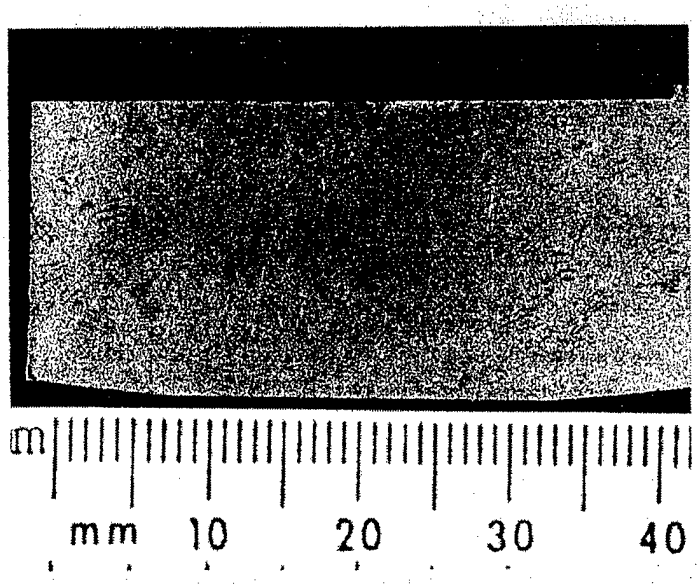

Figure 14. Surface of Vacrosil after EDM.

Figure 15. Close up of lines made by EDM (Vilella's etch).

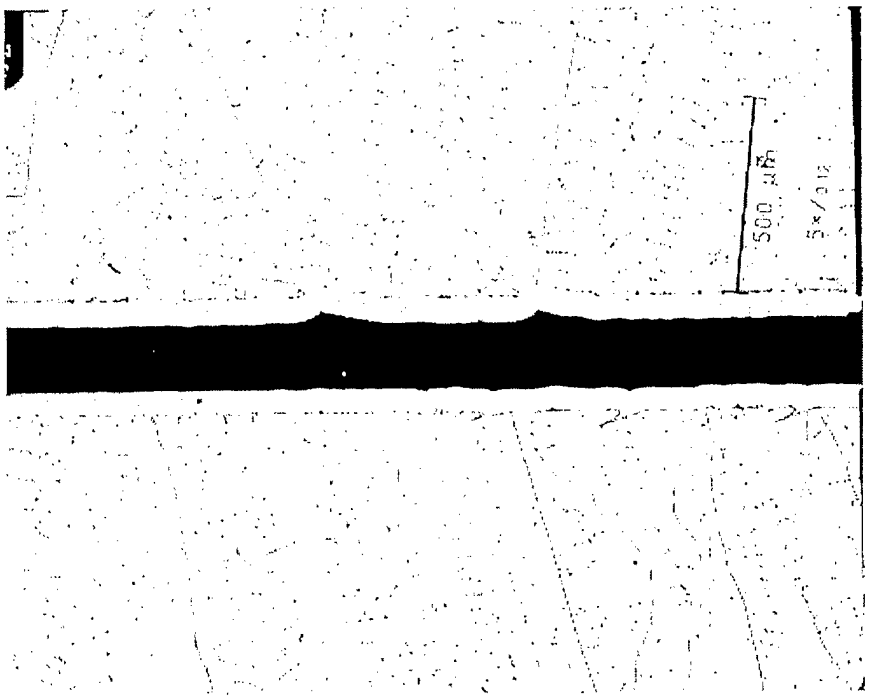

Figure 16. Cross-section of area on Vacrosil after EDM which shows depth of marks from EDM.

TEST PROCEDURES USED IN ROUND ROBIN PROGRAM

Ten tests were completed on various apparatus. Test type and test parameters are summarized in Table 3. Details of tests are more fully explained in forthcoming sections.

Table 3. Completed Damping Tests.

Test Designation	Type of Test	Frequency (Hz)	Strain Range ($\mu\varepsilon$)
A	Cantilevered vibration decay	54.4, 61.7	0.4 - 30
B	Cantilevered vibration decay	785 to 795, 862	3 - 62
C	Torsional vibration decay	0.5	15 - 540
D	Cantilevered resonance	244 to 283	0.5 - 400
E	Fixed guided resonance	30, 35	60 - 1160
F	Axial resonance	40,000	0.4 - 40
G	Torsional resonance vibration	1	0.3 - 51
H	Fixed guided sub-harmonic forced oscillation	0.01, 0.1, and 1	293 - 660
I	Fixed guided sub-harmonic forced oscillation	0.1, 1, 10	49 - 277
J	Double cantilever	0.5, 0.1, 0.05 and 0.01	150 $\mu\varepsilon$ – 1000

Curve-fitting of specimen damping results was done on the PC with TableCurve™ 2D software (originally released through Jandel Scientific, now distributed by SPSS Science). Deconvolution was accomplished using Eqs. (3) through (6), as appropriate. For deconvolution of torsion, cantilever, and fixed-guided data, the derivatives required for Eqs. (4-6) were computed by the TableCurve software. Analysis of the single set of data from longitudinal

oscillations involved curve-fitting of measured data, followed by substitution of the curve-fit formula into Eq. (3), and subsequent calculus necessary for determination of the intrinsic damping.

FLEXUAL VIBRATION DECAY TESTS

Method A used a cantilevered sample inside a vacuum chamber. A wave form generator and amplifier was used to drive an electromagnetic transducer that excited the beam at its natural frequency. A laser vibrometer was used to detect the vibrations of the cantilevered beam specimen. After steady state at the natural frequency and desired amplitude was achieved the current to the excitation transducer was interrupted. The free vibration decay of the specimen, as detected by the laser vibrometer, was recorded in digital form by an oscilloscope, which subsequently determined the peak voltages of the waveform. In order to characterize the strain dependence of damping, the decay profile was divided into blocks of several cycles, and the damping in each block was determined using a modified logarithmic decrement method as described on page 11. The frequency used in Vacrosil tests was 54.4 Hz over a stain range of 0.4 με to 30 με. The frequency used in tests on the HY-100 steel sample was 61.7 Hz. The measurements, the curve fit and the calculated intrinsic damping are shown in Figure 17.

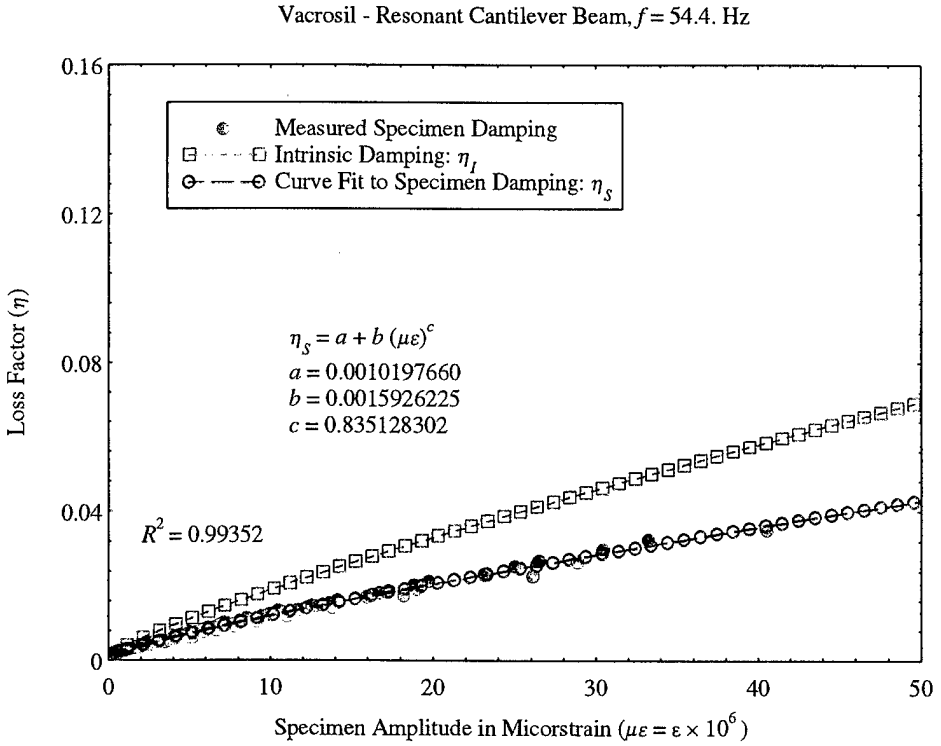

Figure 17. Damping measurements of Vacrosil made by method A.

Method B was performed using a AE0011 Acoustic Elastometer manufactured by Vibran Technologies Inc. Samples were driven to vibrate by a magnetic coil. A feed back loop was used in the instrument to vibrate the sample automatically at its resonant frequency with a constant amplitude controlled by AGC circuit. Changing the receiver gain varied the magnitude of the vibration amplitude. The vibration signal was processed by a data acquisition system and

controlled by a PC-486 computer. The damping was determined by monitoring the free decay of the vibration amplitude after the signal processing unit turned off the exciting magnetic field. During the free decay over 10,000 cycles, signal data was sampled and used to calculate the damping. The measurement errors for the damping and resonance frequency are less that 2% and 0.01% respectively. The capacitance between the sample and an electrode was used as the sensor for the displacement of the vibrating sample. The distance of the capacitor electrodes could be varied by means of a micrometer. This variation of the capacitance changes the frequency, f, of the oscillator, and the relationship of the distance, x, and the oscillator frequency yields the sensitivity of the transducer, $S = \Delta f/\Delta x$. The vibrating sample produces a FM signal at the output of the oscillator. This FM signal is demodulated, with a transfer factor of $S_d = \Delta V/\Delta f$ = 0.89 mV/kHz. The demodulated LF signal represents the vibration of the sample, it has the frequency of the vibrating samples and an amplitude proportional to the displacement amplitude of the sample. A preamplifier with specified gain, G, amplified this LF signal. During the measurement, the output amplitude of the preamplifier was kept to a constant value of 8 volts, controlled by a AGC circuit. The vibration amplitude of the sample is given by the equation

$$\Delta X_{pp} = \frac{V}{GS_cS_d}$$

The frequencies used varied between 785 to 795 Hz over a strain range of 3 με - 62 με. The measurements, the curve fit and the calculated intrinsic damping are shown in Figure 18.

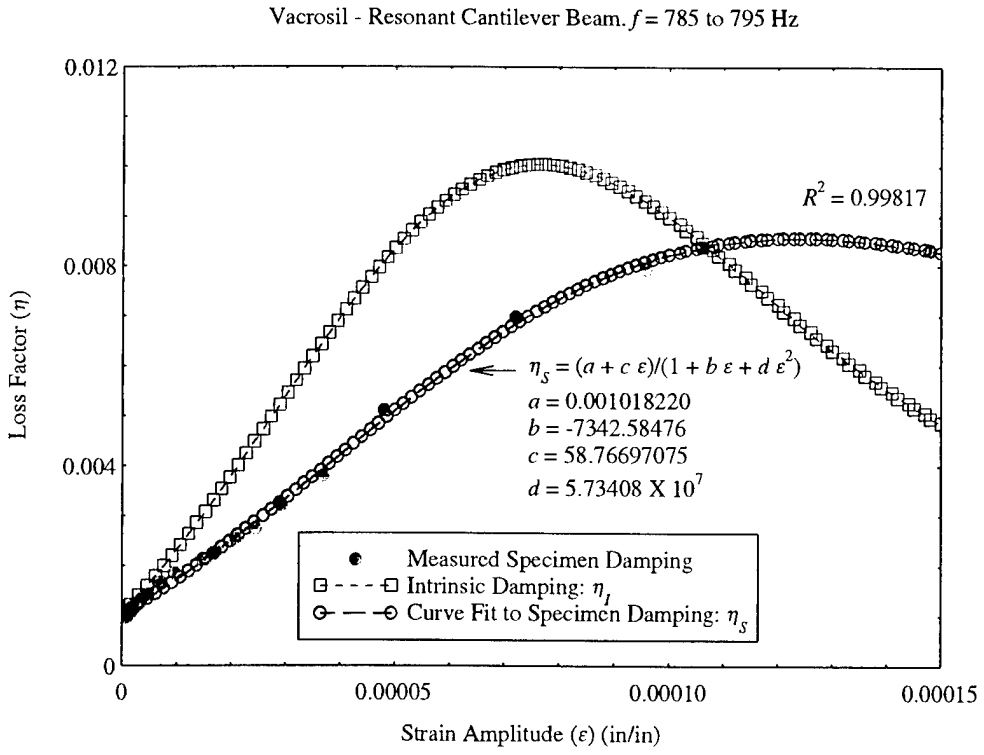

Figure 18. Damping measurements of Vacrosil made by method B.

TORSIONAL VIBRATION DECAY TEST

Method C was performed using an inverted torsion pendulum. The pendulum is excited electromagnetically to the strain amplitude of about 10^{-6} and then allowed to oscillate freely. Contactless inductive displacement sensors measure the sample's response. Computer fitting of the damping sinusoidal curve obtains the loss factor and frequency values. The frequency used was 0.5 Hz. The measurements, the curve fit, and the calculated intrinsic damping are shown in Figure 19.

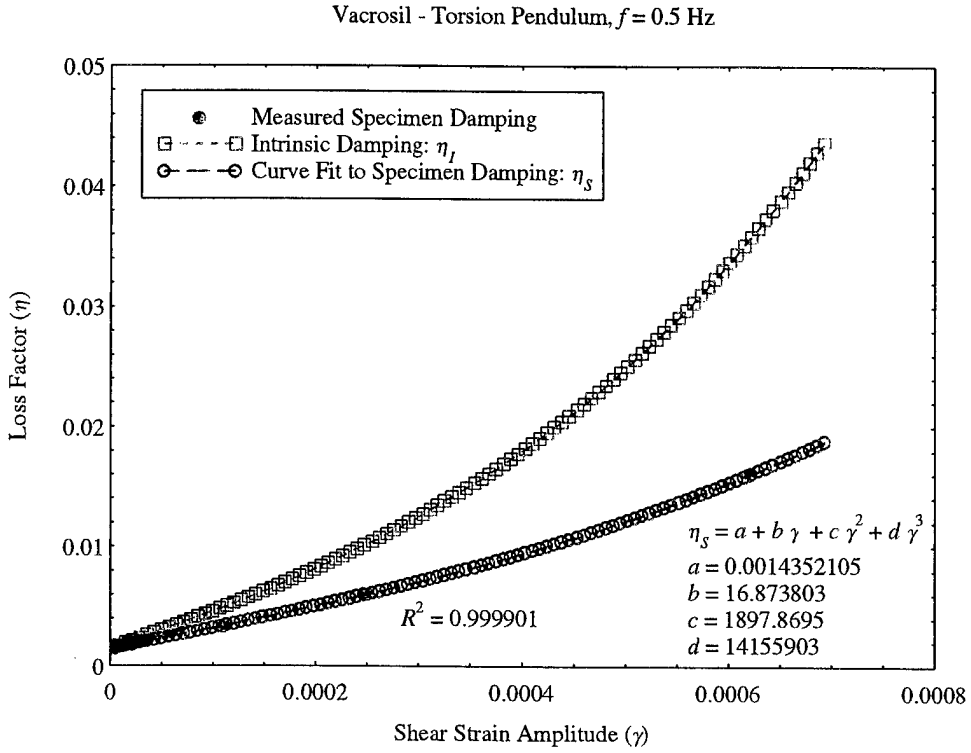

Figure 19. Damping measurements of Vacrosil made by method C.

RESONANT BEAM TEST

Method D was performed using a cantilever beam of triangular shape. A swept-sine technique was used to excite the specimen at the tip, and the strain was measured with a strain gauge at the root of the beam. The frequencies used were 244 Hz for HY 100 steel and 283 Hz for Vacrosil, over a strain range of 0.5 με to 400 με. The measurements, the curve fit, and the calculated intrinsic damping are shown in Figure 20.

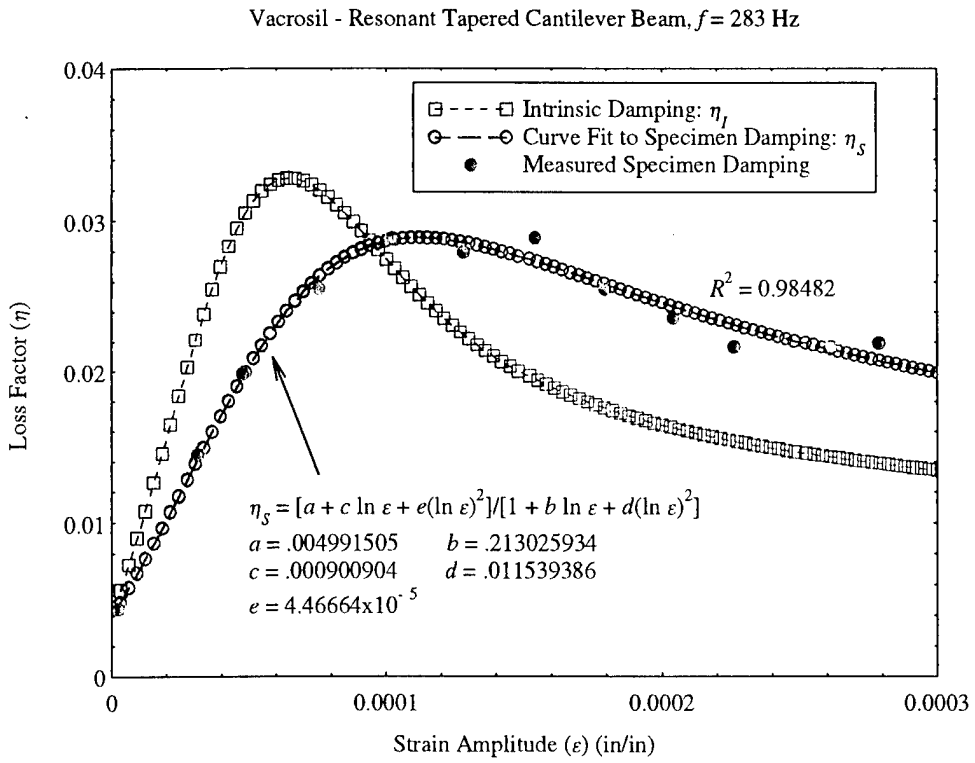

Figure 20. Damping measurements of Vacrosil made by method D.

Method E was performed using the DuPont DMA 983 operated at resonance. The sample and fixturing arms form a compound resonance system. The sample is displaced and set into oscillation. Normally, a system so displaced would oscillate at the system's resonant frequency, with constantly decreasing amplitude due to the loss of energy within the sample. The amplitude signal from the LVDT is used to control the output signal of the electromechanical driver. The driver supplies additional energy to the driven arm forcing the coupled system to oscillate at constant amplitude. The frequency of oscillation is directly related to the stiffness or storage modulus of the sample under investigation, while the energy needed to maintain constant oscillation amplitude is a measure of the damping within the sample. Because sample flexure actually extends beyond the clamp face into the center of the clamps, the sample length measured must be corrected to reflect this extension of the real sample length. The length correction is a term that is added to the measured sample length to correct for this extension. The length correction is determined by the following method. The elastic modulus at room temperature is accurately measured by other means. Based on those values a length correction for the DMA software is adapted such that an equal value for the modulus was obtained by the DMA measurements. The required length correction varies somewhat with the stiffness of the material. Measurements were made at a frequency between 30 to 35 Hz over a strain range of 60 $\mu\varepsilon$ – 1160 $\mu\varepsilon$. The measurements, the curve fit and the calculated intrinsic damping are shown in Figure 21.

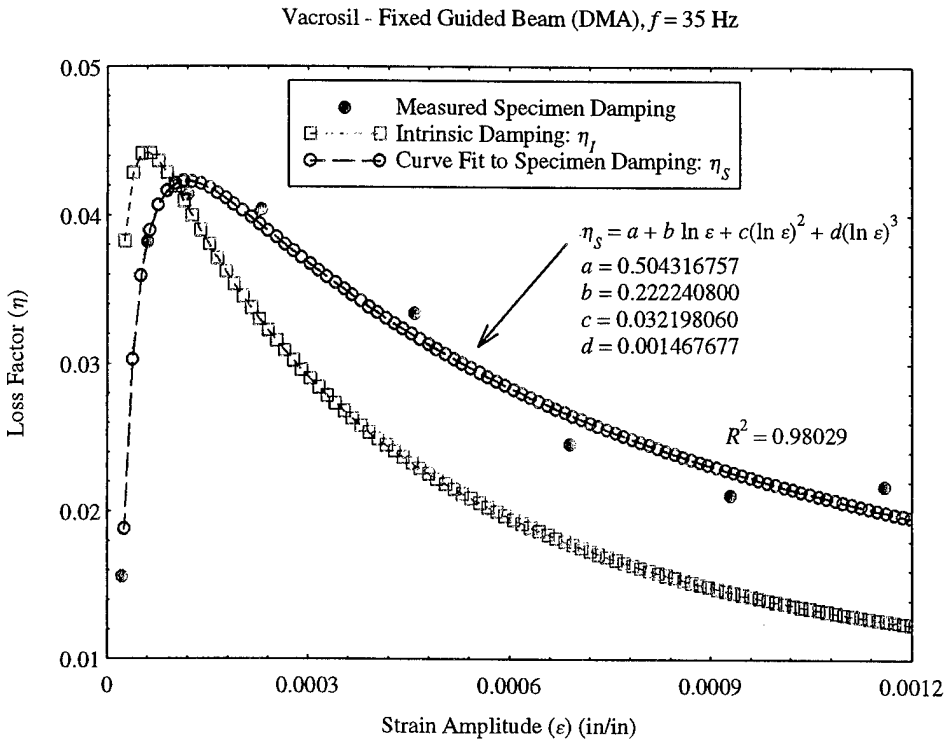

Figure 21. Damping measurements of Vacrosil made by method E.

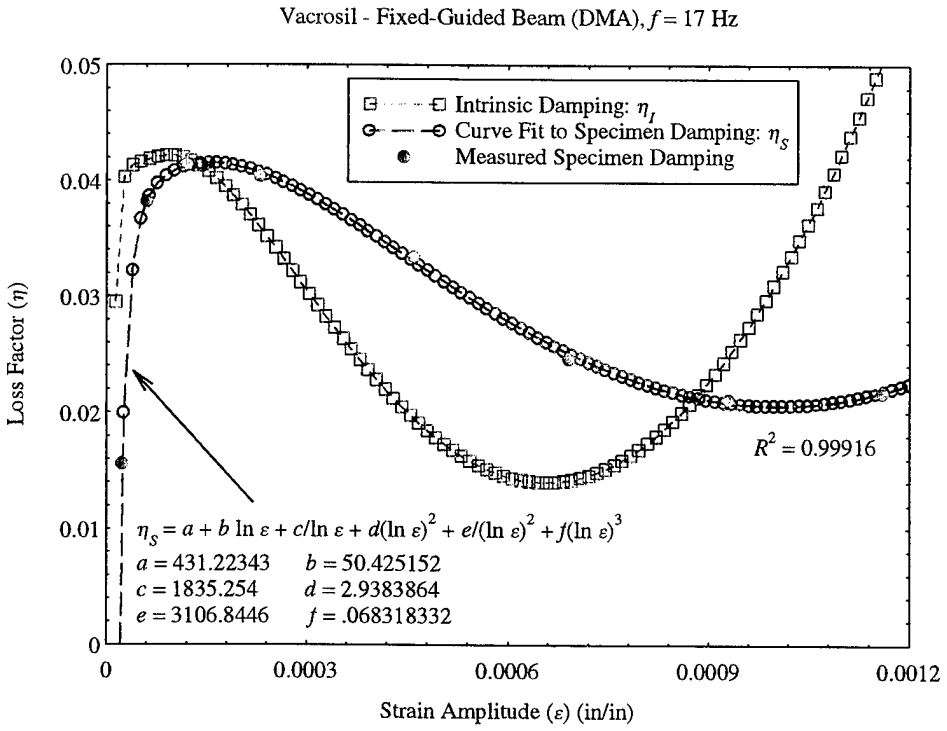

Figure 22. Alternative Curve Fit Applied to the Results of Method E

One must be careful, however, to make an appropriate choice for curve fitting. As shown in Figure 22, even though one curve fit to the data might be statistically better (higher R^2) than another, deconvolution to intrinsic damping could lead to a counterintuitive result. The counterintuitive behavior in Figure 22 is seen as rising values of intrinsic damping above the strain level of 0.0007. For this reason, only the data from Figure 21 were used in overall comparisons of results from the round robin.

AXIAL RESONANT TEST

Method F was performed using a PUCOT (pulsed ultrasonic composite oscillator technique). A quartz piezoelectric bar (the drive crystal) was cemented to a second identical crystal (the gage crystal). Chromel wires supported each crystal. A closed loop crystal driver was used to generate and monitor drive and gage voltages. A voltage was applied across the drive crystal using the closed loop crystal driver. This drive voltage was minimized while the gage voltage was maximized to ensure that the system was resonating. The period of the specimen was then evaluated and compared to the period of the piezoelectric crystals. If the ratio between the two was within 5% of unity the data was kept. If the ratio was not within this range then the length of the specimen was changed and the system reassembled and tested again. The frequency used was 40 K Hz over a strain range of 0.4 με to 40 με. The measurements, the curve fit and the calculated intrinsic damping are shown in Figure 23. See Appendix A for a detailed derivation of the intrinsic damping equation.

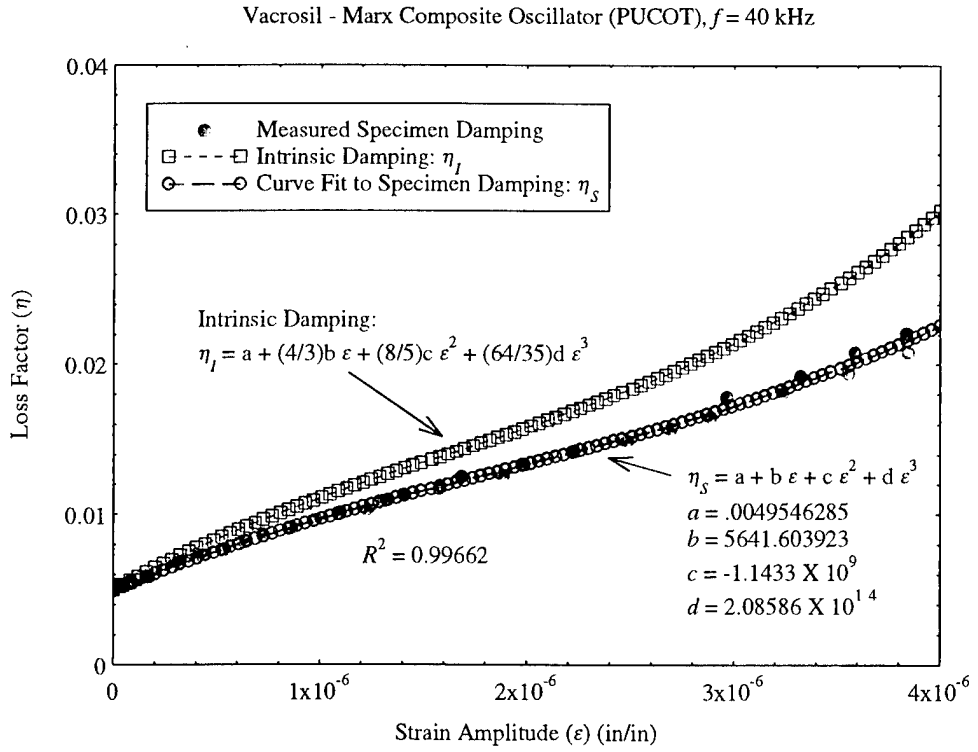

Figure 23. Damping measurements of Vacrosil made by method F.

TORSIONAL RESONANT TEST

Method G was performed using a Metravib inverted Torsion pendulum. The test piece is the return element of a compensated inverted torsional pendulum whose moment of inertia is very low. The torque created by the interaction between a magnet and the Helmholtz coils carrying a current is transmitted to the test piece by a high rigidity rod. The sample strain is detected by a light beam, supplied by a controlled source and reflected by a mirror that is attached by a rigid rod, toward a differential photovoltaic cell. A low drift amplifier supplies a voltage in proportion with the strain on the test piece. The suspension system wire pulley and counter weight removes any axial load on the sample. A damper lowers the effect of parasitic vibrations induced by the surroundings. The frequency used was 1 Hz over a strain range of 0.3 με - 51 με.

The measurements, the curve fit and the calculated intrinsic damping from two separate curve fit formulas are shown in Figure 24 and Figure 25. It is interesting to note that the two different curve fit equations produce the same intrinsic damping result. This is due to the fact that there is a sufficient number of data points over a wide range of strain to describe a well defined trend (in this case a peak). The data from this set thus permits a repeatable damping vs. strain curve for multiple curve-fits.

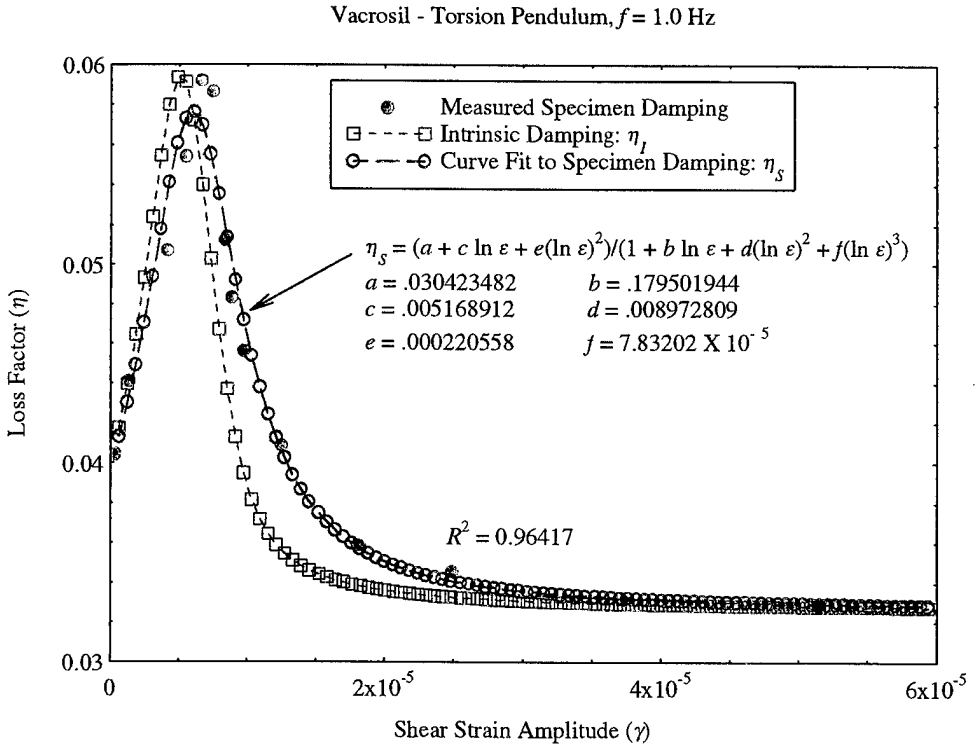

Figure 24. Damping measurements of Vacrosil made by method G with natural log curve-fit.

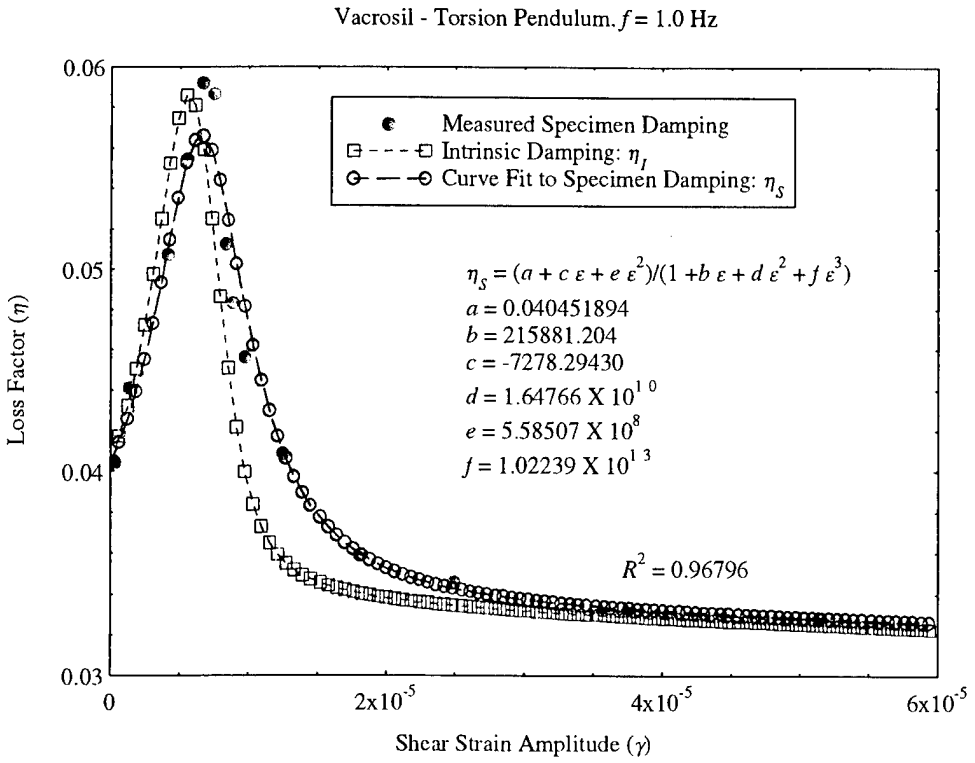

Figure 25. Damping measurements of Vacrosil made by method G with a polynomial curve fit.

SUB-HARMONIC FORCED OSCILLATION OF BEAMS

Method H was also performed using the DuPont DMA 983, this time operated below the resonance frequency. This method used a cantilever sample driven at fixed frequencies and directly measures the phase angle between the applied load and the measured displacement. The measurements were taken at three distinct frequencies, 0.01, 0.1, and 1 Hz over a strain range of 293 με to 660 με. The measurements, the curve fit, and the calculated intrinsic damping are shown in Figure 26; results were nearly identical for the three frequencies. Results shown in Figure 26 are for f = 0.1 Hz. The linear curve fit formula identified on the plot of Figure 26 produced the most reasonable result for intrinsic damping. Efforts to analyze the data using higher order curve fit formulae led to counterintuitive intrinsic damping results.

Method I was performed using DMTA equipment manufactured by Rheometric Scientific. This method also used a cantilever sample driven at fixed frequencies and directly measures the phase angle between the applied load the measured displacement. The measurements were taken at three fixed frequencies, 0.1, 1, 10 Hz, over a strain range of and 49 με to 277 με. The measurements, the curve fit and the calculated intrinsic damping are shown in Figure 27, for the case of f = 10 Hz.

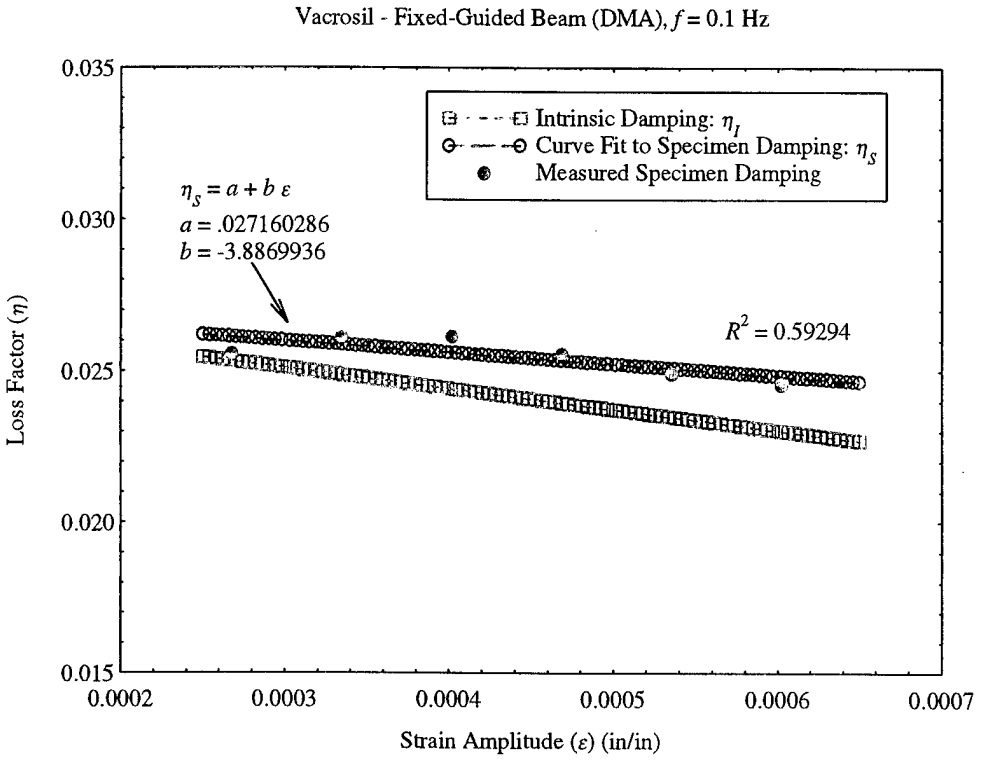

Figure 26. Damping measurements of Vacrosil made by method H.

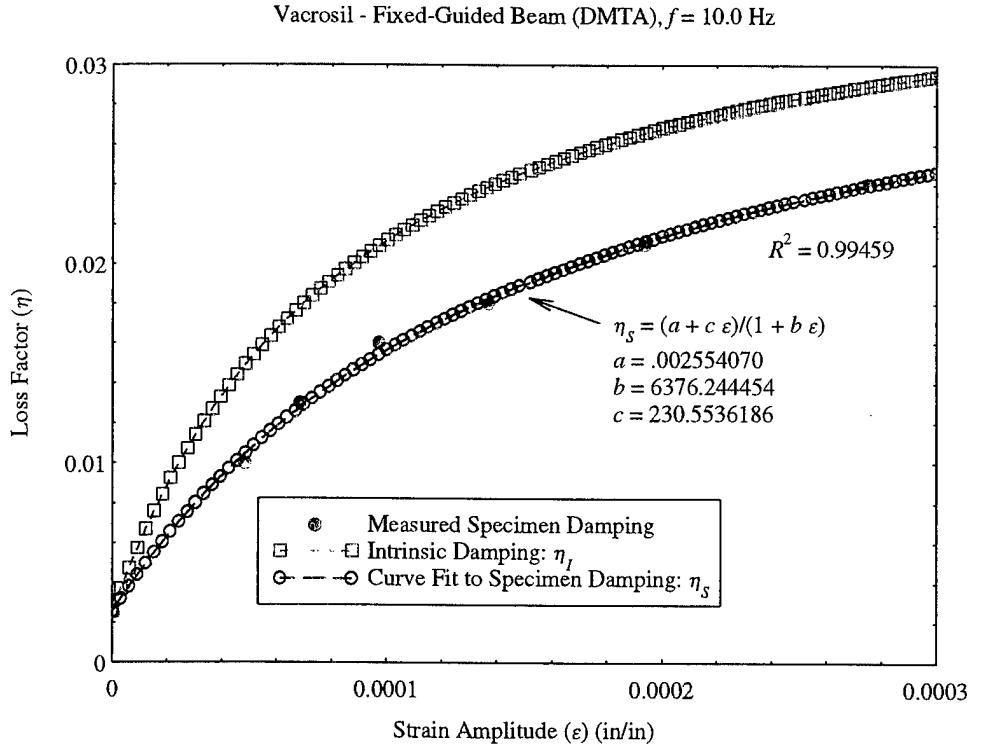

Figure 27. Damping measurements of Vacrosil made by method I.

Method J was performed using a flexion double cantilever apparatus at frequencies of 0.5, 0.1, 0.05 and 0.01 Hz over a strain range of 150 $\mu\varepsilon$ – 1000 $\mu\varepsilon$. Data samples are reported for increasing increments of strain. The measurements, the curve fit and the calculated intrinsic damping are shown in Figure 28. A second curve-fit analysis is shown in Figure 29. Damping results from the different frequency tests are generally indistinguishable, and were therefore grouped together. The curve-fit process on the first data set, shown in Figure 28, assumed a data point at the origin. Another curve-fit equation, shown in Figure 29, which excluded the origin produced similar results upon deconvolution to intrinsic damping, but only within the strain limits of $\varepsilon = 0.0002$ to $\varepsilon = 0.0007$. Above this strain, the deconvolved result becomes counterintuitive. It is again emphasized that the equations must be carefully fit to the data so that counterintuitive results are avoided. The simple linear equation that is used to fit the data in Figure 28 has a reasonably high correlation coefficient and captures the main trend of the data. However, upon deconvolution to intrinsic damping, the deconvolved result indicates that damping will be negative for strains higher than 0.00082, which is physically impossible. In the next section there will be compilation and comparison of all round-robin results. For the purposes of comparing method J to the other test results, the data shown in Figure 28 will be used, while that of Figure 29 will not.

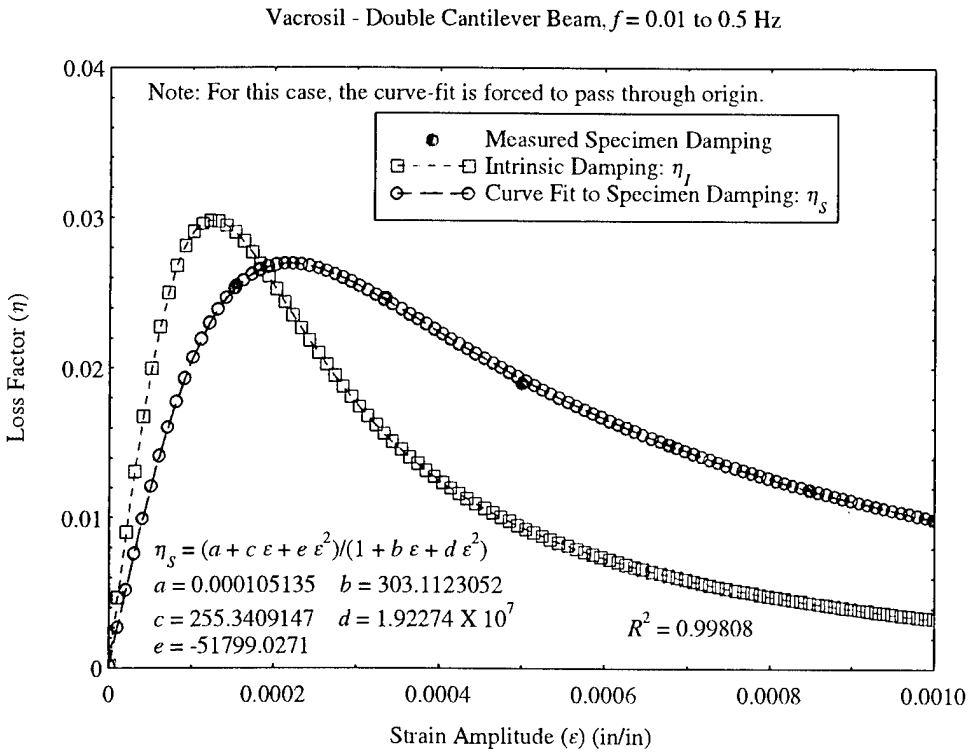

Figure 28. Damping measurements of Vacrosil made by method J with a polynomial curve fit forced through zero.

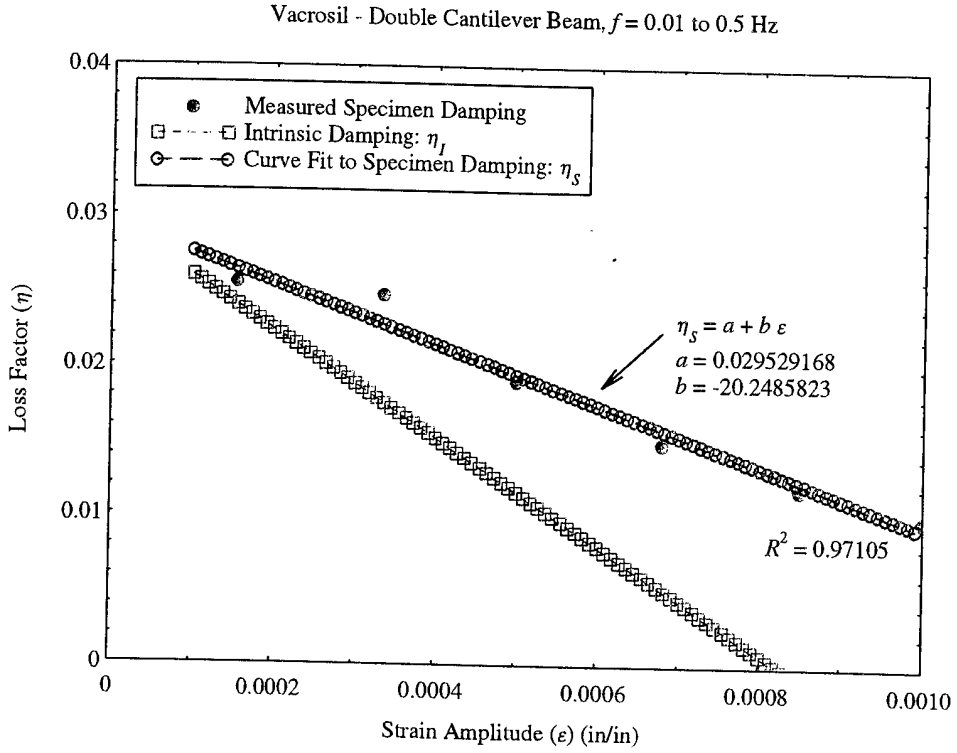

Figure 29. Damping measurement of Vacrosil by method J and linear curve fit.

RESULTS AND DISCUSSION

A summary plot of results for the damping measurements for Vacrosil and HY-100 are shown in Figure 30 and Figure 31 respectively. Deconvolved intrinsic damping curves for Vacrosil are shown in Figure 32. In general, if there was a sufficient number of data and a well developed curve, then the curve fitting led to repeatable values of calculated intrinsic damping. But, if there were insufficient data or if the trend of the data was not clear, then the choice of curve fit equation was seen to greatly affect the computed values of intrinsic damping.

On considering the summary plot of results for Vacrosil (Figure 30), it is evident that the results are spread over a wide range. The differences in the data measured with disparate test methods are far wider than originally expected. Evaluation of Vacrosil results following deconvolution to intrinsic damping (as shown in Figure 32) does not help in the correlation of results because the correction is much smaller than the errors in measurement. Possible reasons for the large range of damping values include both inaccurate determinations of strain, as well as biasing sources of damping from the test system which was used. Neither of these can be quantified without further work.

The damping results from tests on HY-100 steel are somewhat more consistent. Some of the test results show strain dependence and high damping for HY-100, a feature which has not been shown before and may be in error.

The Young's modulus data for Vacrosil and HY-100 are presented in Figure 33 and Figure 34 respectively. Based on the HY-100 results, the modulus results produced by methods H and I are judged to be inaccurate. The length corrections used in the DMA test of Method E were determined by measuring the modulus with an independent method. Thus the data was constrained to produce that modulus data. Although this is apparently an excellent way to obtain

accurate damping data from DMA's and DMTA's, it illustrates the inability of this method to independently measure the modulus of stiff materials.

One final note regarding results from torsion tests. Torsion test samples in the round-robin program were made with a square cross-section. To meet time and schedule requirements, torsion test results were post-processed using Eq. (4), which is derived for the case of circular cross-section. Therefore, intrinsic damping results presented for torsion tests are not strictly precise. The post-processed results are a first approximation of intrinsic damping, however. Due to the existence of a wide spread in the collective set of data, this approximation is deemed reasonable for the purposes of this report. If better precision is desired in torsion tests with square samples, the post-processing method of Roatta et al [13] should be used.

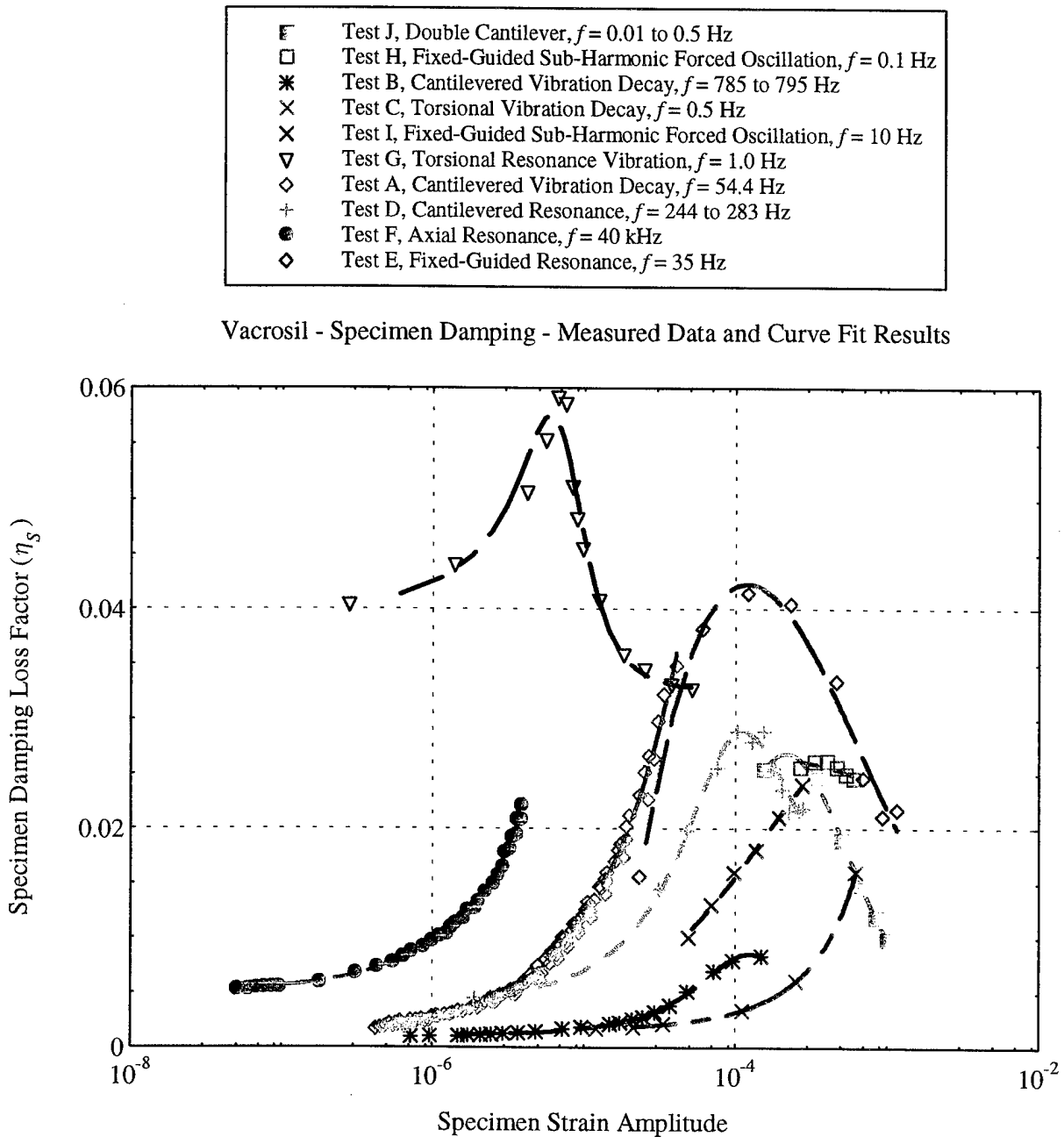

Figure 30. Results of damping tests on Vacrosil.

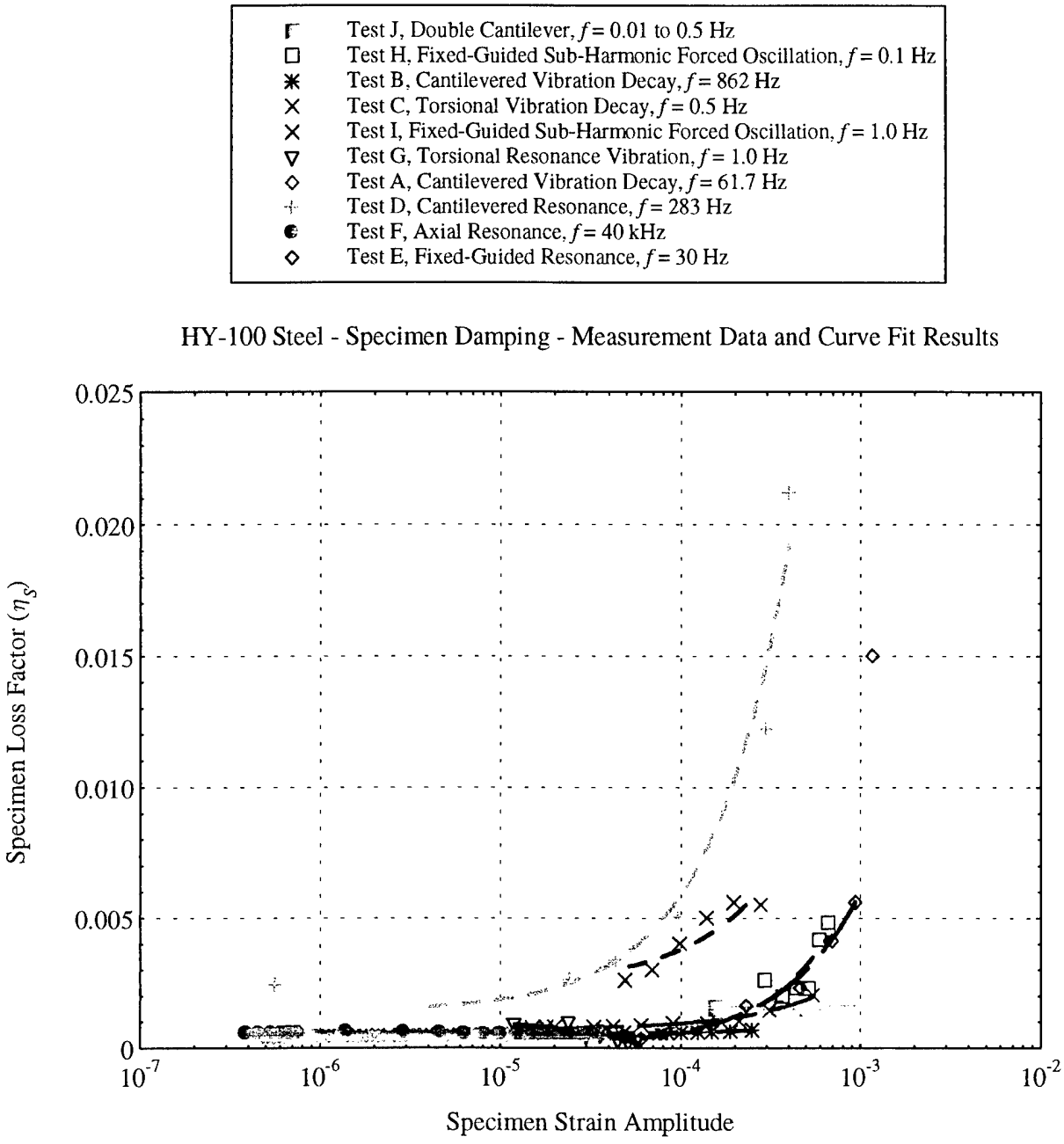

Figure 31. Results of damping tests on HY-100.

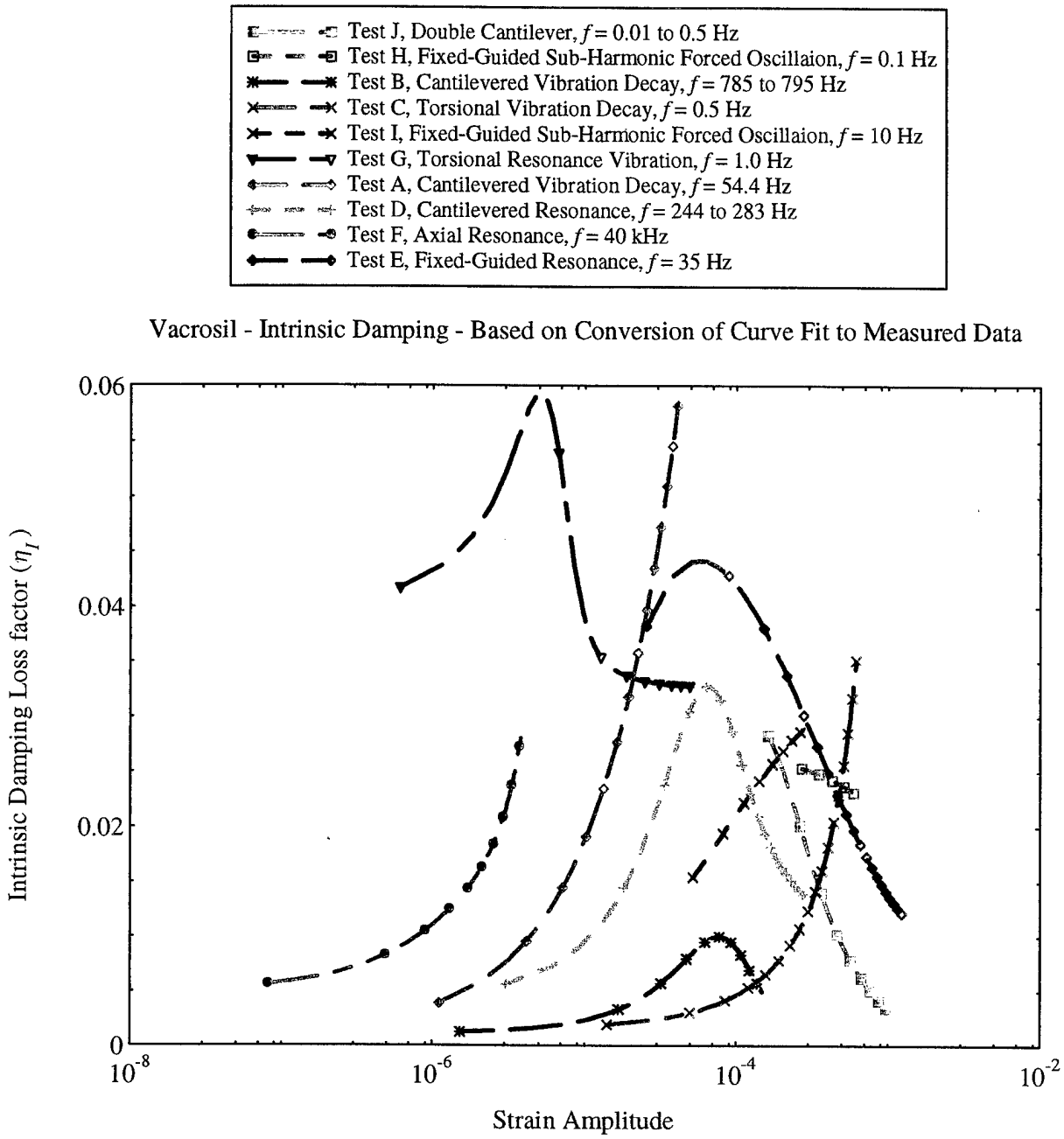

Figure 32. Intrinsic damping of Vacrosil calculated from each method.

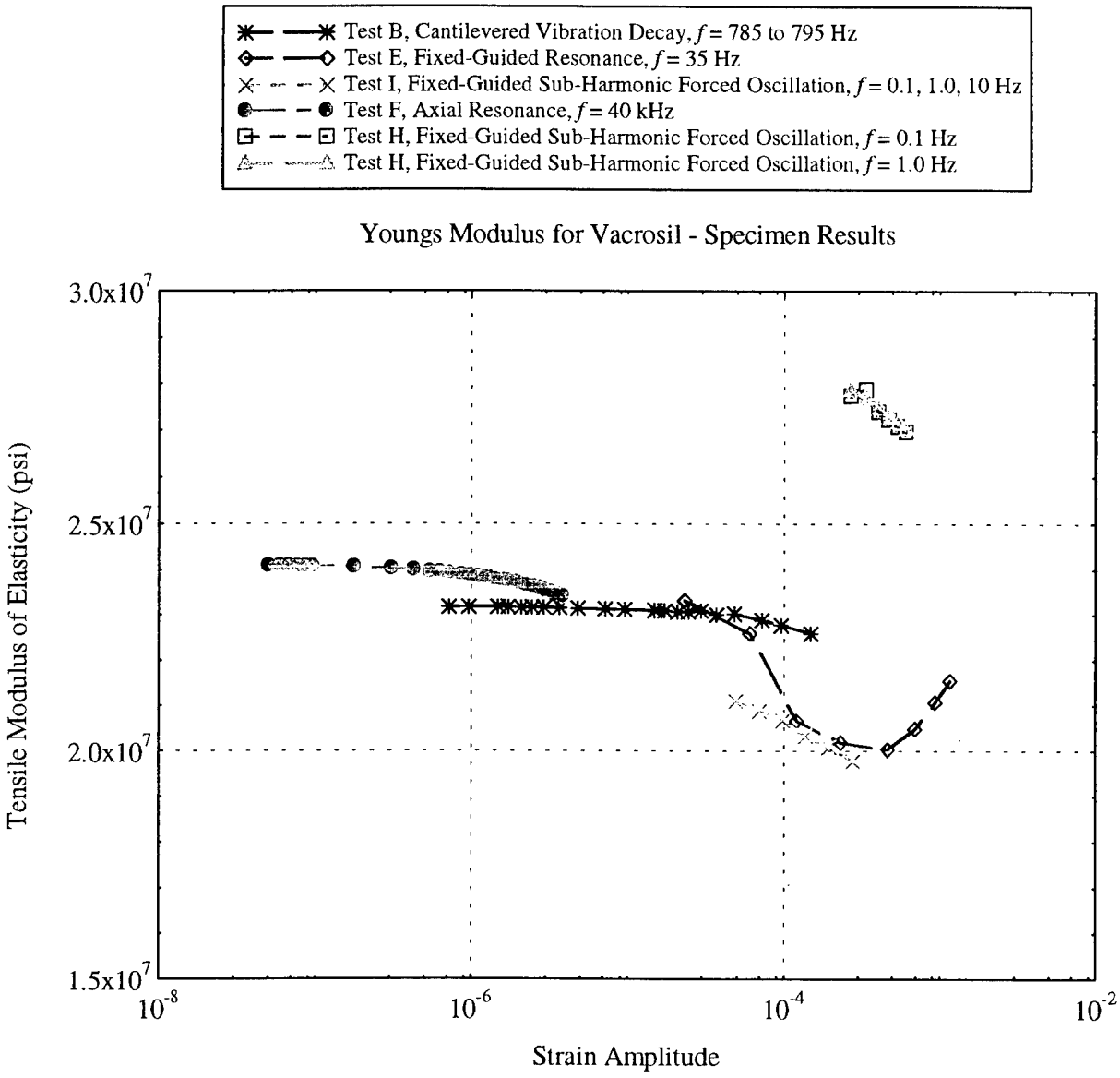

Figure 33. Young's modulus measured on Vacrosil.

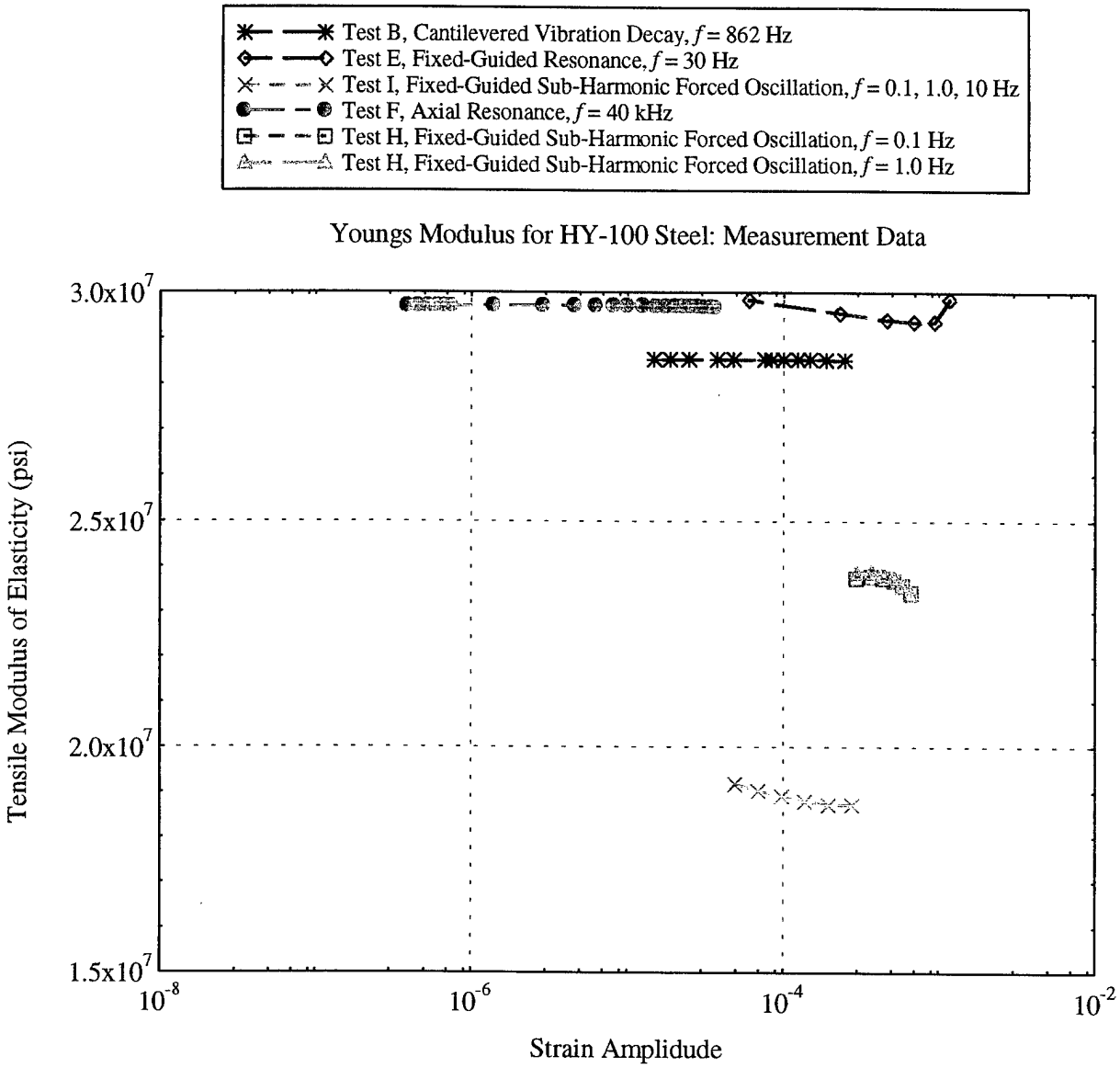

Figure 34. Young's modulus measured on HY-100.

SUMMARY

Results of the round-robin program indicate that more work will be needed to enable a good standard for measuring material damping in metals and stiff composites. Both a standard method for measuring stiff, linear, low-damping materials and a standard method for measuring strain dependent intrinsic damping in stiff, nonlinear, high damping materials must be established. The standard for nonlinear damping measurements should necessarily employ deconvolution from specimen damping to intrinsic damping. It should also reconcile the difference in strain measures that result from axial tests (a combination of dilitation and distortion) and torsion tests (pure distortion). The possible effect of frequency, which is often ignored as a variable in intrinsic damping of metals, should also be considered as part of any proposed standard.

The magnitude of damping values presented on the round-robin summary plot for Vacrosil showed significant differences in damping levels and trends. Likely reasons include inaccurate measurement of specimen strain amplitude, and/or biasing sources of damping from the measurement system. Calculation of intrinsic damping did not improve the agreement of Vacrosil results, due to the gross spread of the data.

The agreement of the damping measurement of HY-100 values was better, but not ideal. Most measurements showed that HY-100 was not strain dependent at strains less than 10 $\mu\varepsilon$, but a few methods indicated some strain dependence above that level. Without further work there is no way to know if the strain dependence shown for HY-100 steel is a real property, or the artifact of biasing sources from the test apparatus. The latter reason is not unlikely.

The modulus data for HY-100 steel and Vacrosil show considerably better agreement, possibly because the modulus varies less with strain. However, not all investigators were set up to record modulus, so the set of data is not complete. Two modulus results for HY-100 are clearly inaccurate, these results were from DMTA and DMA machines. Because of the recognized limitations of these machines to accurately measure the modulus of stiff materials, it is recommended that the modulus be measured on a separate apparatus and that value be used to find the length correction in order to improve the accuracy of the damping measurements

Results from this round-robin exercise demonstrate that damping in metals is difficult to measure on a repeatable and reliable basis, when using different methods of testing. For many common structural metals, damping is so low that it can be difficult to distinguish from background noise. On the other hand, for special metals with high damping, the damping may be strain dependent. The fact that strain is not homogeneous in the test specimen further complicates measurements on materials with strain dependent features. It is clear that further work is necessary if material damping measurements are to be made on a reliable basis. Any future damping standard should probably be linked with standard procedures for measuring modulus, thereby increasing confidence in the procedure.

REFERENCES

1. Gibson, R.F., "Nontraditional Applications of Damping Measurements," *Special Technical Publication 1169: Mechanics and Mechanisms of Material Damping*, ASTM, edited by A. Wolfenden and V.K. Kinra, 60-75 (1992)

2. Willertz, L.E., "Magnetomechanical Damping Properties of AISI 403 Stainless Steel with Applied Static Torsional and Axial Stresses," *Journal of Testing and Evaluation*, 2 [6], 478-82 (1974)

3. Dew, D., "Strain Dependent Damping Characteristics of a High Damping Manganese-Copper Alloy," Report No. NPS69-86-007, Naval Postgraduate School, Monterey, California, September, (1986)

4 . Perkins, A.J., G.R. Edwards, and N.A. Hills, "Material Approaches to Ship Silencing, "Report no. NPS-59PS74061, u.s. Naval Postgraduate School, Monterey, CA, (1974)

5. Schetky, L.M. and J. Perkins, "The 'Quiet' Alloys," *Machine Design*, 202-06 (April 6, 1978)

6. Schneider, W., P. Schrey, G. Hausch, and E. Torok, "Damping Capacity of Fe-Cr and Fe-Cr Based High Damping Alloys," *Journal De Physique*, Colloque C5, 42 [10], [October] C5-635 through C5-639 (1981)

7. Masumoto, M., M. Hinai, and S. Sawaya, "Damping Capacity and Pitting Corrosion Resistance of Fe-Mo-Cr Alloys," *Transactions of the Japan Institute of Metals*, 25 [12], 891-99 (1984)

8. Nippon Kokan K.K., Tranqaloy Data Sheets (1981)

9. Kawabe, H. and K. Kuwahara, "A Consideration of the Strain Dependent Damping and Modulus in Ferromagnetic Metals," *Transactions of the Japan Institute of Metals*, 22 [5], 301-08 (1981)

10. Povolo, F. and R. Gibala, "Internal Friction and Modulus Defect of Materials Subjected to Inhomogenous Stresses," *Philosophical Magazine*, 27 [6], 1281-88 (1973)

11. Sprungmann, K.W. and I.G. Ritchie, "Instrumentation, Computer Software and Experimental Techniques Used in Low-Frequency Internal Friction Studies at WNRE," Technical Report AECL-6438, Atomic Energy of Canada Limited, Whiteshell Nuclear Research Establishment, Pinawa, Manitoba, Canada, (1980).

12. Molinas, B.J. and F. Povolo, "Analysis of the Problem of Converting Measured Amplitude-Dependent Internal Friction to Intrinsic Values. Detailed Study of the Case of Forced Oscillations," *Journal of Physics E: Scientific Instrumentation*, 20, 970-77 (1987)

13. Roatta, A., B.J. Molinas, and C.N. Tomé, "A Method to Deconvolute Amplitude Dependent Internal Friction Data: Theory and Experiment," *Philosophical Magazine A*, 67 [1], 87-97 (1993)

14. Graesser. E.J. and C.R. Wong, "A Proposed Correlation Technique for Strain Dependent Damping Measurements," *Damping of Multiphase Inorganic Materials*, edited by R. Bhagat, ASM International, Materials Park, Ohio, 61-72. (1992)

15. Cochardt, A.W., "The Origin of Damping in High-Strength Ferromagnetic Alloys," Trans. ASME, *Journal of Applied Mechanics*, 75 [June], A-196 through A-200 (1953)

16. Smith, G.W. and J.R. Birchak, "Effect of Internal Stress Distribution on Magnetomechanical Damping," *Journal of Applied Physics*, 39 [5], 2311-16 (1968)

17. Ritchie, I.G., and Z.-L. Pan, "Characterization of Damping Properties of High Damping Alloys," *Special Technical Publication 1169: Mechanics and Mechanisms of Material Damping*, ASTM, edited by A. Wolfenden and V.K. Kinra, 142-57 (1992)

18. Marx, J., "Use of the Piezoelectric Gauge for Internal Friction Measurements," The Review of Scientific Instruments, 22 [7], 503-09, (1951)

19. Povolo, F., "Corrections due to Inhomogeneous Strains to the Internal Friction Measured in Free Decay," *Scripta Metallurgica*, 16 [7], 885-90 (1982)

20. Ritchie, I.G., C.H. Woo, and K.W. Sprungmann, "Comments on the Corrections due to Inhomogeneous Strains to the Internal Friction Measured in Free Decay," *Scripta Metallurgica*, 16 [7], 891-94 (1982)

21. Kinra, V.K., G.G. Wren, S.P. Rawal and M.S. Misra, "On the Influence of Ply-Angle on Damping and Modulus of Elasticity of a Metal-Matrix Composite," *Metallurgical Transactions A*, , 22A [3], 641-51 (1991)

22. Ewins, D.J., *Modal Testing: Theory and Practice*, Research Studies Press Ltd., John Wiley and Sons Inc., 181-192. (1984)

23. Graesser. E.J. and C.R. Wong, "The Relationship of Traditional Damping Measures for Materials with High Damping Capacity," *Special Technical Publication 1169: Mechanics and Mechanisms of Material Damping*, Ed. by R. Bhagat, American Society for Testing and Materials, edited by A. Wolfenden and V.K. Kinra, , 316-343. (1992)

APPENDIX A: CONVERSION RELATION FOR LONGITUDINAL SPECIMEN TEST WITH POLYNOMIAL FIT TO MEASURED DATA

For the case of resonant (first mode) longitudinal oscillations in a bar of material with strain dependent damping properties, the amplitude dependent intrinsic damping is related to specimen damping by the following formula [10]:

$$\eta(\varepsilon) = \frac{1}{2}\frac{1}{\sqrt{\varepsilon}}\frac{d}{d\varepsilon}\left\{\int_0^{\varepsilon}\frac{\eta_s(\varepsilon_0)\varepsilon_0}{\sqrt{\varepsilon-\varepsilon_0}}d\varepsilon_0\right\} \tag{A-1}$$

The damping (loss factor) of the specimen, η_s, is the result of a curve fit to measured data. The curve fit formula for η_s as a function of specimen strain amplitude (ε_0) is inserted into the integral above, and the calculus of Eq. (A-1) is conducted to produce intrinsic damping, η, which is a function on axial strain is ε.

The first step in the conversion process involves curve-fitting of the specimen damping data. The integral is then solved and intrinsic damping evaluated. For the PUCOT results generated in the round-robin program, a third order polynomial was used. The details for determination of intrinsic damping, based on a polynomial curve-fit to specimen results, are given in this appendix.

Let us first simplify notation, as follows:

Let $y = \eta$

$y_s = \eta_s$

$x = \varepsilon$

$\zeta = \varepsilon_0$

Using the new notation, Eq. (A-1) is

$$y(x) = \frac{1}{2}\frac{1}{\sqrt{x}}\frac{d}{dx}\int_0^{x}\frac{y_s(\zeta)\zeta}{\sqrt{x-\zeta}}d\zeta \tag{A-2}$$

PUCOT specimen data was fit with a third-order polynomial:

$$y_s(\zeta) = a + b\zeta + c\zeta^2 + d\zeta^3$$

Substitute y_s into the integral of Eq. (A-2). The integral becomes:

$$\int_0^{x}\frac{y_s(\zeta)\zeta}{\sqrt{x-\zeta}}d\zeta = \int_0^{x}\frac{(a+b\zeta+c\zeta^2+d\zeta^3)\zeta}{\sqrt{x-\zeta}}d\zeta$$

$$\int_0^x \frac{y_s(\zeta)\zeta}{\sqrt{x-\zeta}}d\zeta = a\int_0^x \frac{\zeta}{\sqrt{x-\zeta}}d\zeta + b\int_0^x \frac{\zeta^2}{\sqrt{x-\zeta}}d\zeta + c\int_0^x \frac{\zeta^3}{\sqrt{x-\zeta}}d\zeta + d\int_0^x \frac{\zeta^4}{\sqrt{x-\zeta}}d\zeta \qquad \text{(A-3)}$$

The problem will involve solution of the above four integrals. The following integral solution is available from calculus:

$$\int \frac{u^n du}{\sqrt{a+bu}}du = \frac{2u^n\sqrt{a+bu}}{(2n+1)b} - \frac{2na}{(2n+1)b}\int \frac{u^{n+1}du}{\sqrt{a+bu}}$$

The first integral on the right hand side of Eq. (A-3) is evaluated below.

$$\int_0^x \frac{\zeta}{\sqrt{x-\zeta}}d\zeta = \frac{2\zeta\sqrt{x-\zeta}}{3(-1)}\Bigg|_0^x - \frac{2x}{3(-1)}\int_0^x \frac{d\zeta}{\sqrt{x-\zeta}}$$

$$\int \frac{du}{\sqrt{a+bu}} = \frac{2\sqrt{a+bu}}{6}$$

$$\Rightarrow \int_0^x \frac{d\zeta}{\sqrt{x-\zeta}} = \frac{2\sqrt{x-\zeta}}{-1}\Bigg|_0^x$$

$$= -2\left[\sqrt{x-x} - \sqrt{x-0}\right] = 2\sqrt{x}$$

$$\frac{2\zeta\sqrt{x-\zeta}}{3(-1)}\Bigg|_0^x = -\frac{1}{3}\left[2x\sqrt{0} - 2\cdot 0\sqrt{x}\right] = 0$$

$$\therefore \int_0^x \frac{\zeta}{\sqrt{x-\zeta}}d\zeta = 0 + \frac{2x}{3}\left(2\sqrt{x}\right) = \frac{4}{3}x^{\frac{3}{2}}$$

The second integral on the right hand side of Eq. (A-3) is evaluated next.

$$\int_0^x \frac{\zeta^2}{\sqrt{x-\zeta}}d\zeta = \frac{2\zeta^2\sqrt{x-\zeta}}{5(-1)}\Bigg|_0^x - \frac{4x}{5(-1)}\underbrace{\int_0^x \frac{\zeta d\zeta}{\sqrt{x-\zeta}}}_{\frac{4}{3}x^{\frac{3}{2}}}$$

$$\frac{2\zeta^2\sqrt{x-\zeta}}{5(-1)}\Bigg|_0^x = -\frac{2}{5}\left[x^2\sqrt{0} - 0^2\sqrt{x}\right] = 0$$

$$\therefore \int_0^x \frac{\zeta^2}{\sqrt{x-\zeta}} d\zeta = \frac{4x}{5} \cdot \frac{4}{3} x^{\frac{3}{2}} = \frac{16}{15} x^{\frac{5}{2}}$$

The third integral on the right hand side of Eq. (A-3) is:

$$\int_0^x \frac{\zeta^3}{\sqrt{x-\zeta}} d\zeta = \frac{2\zeta^3 \sqrt{x-\zeta}}{7(-1)}\Bigg|_0^x - \frac{2(3)x}{7(-1)} \underbrace{\int_0^x \frac{\zeta^2 d\zeta}{\sqrt{x-\zeta}}}_{\frac{16}{15} x^{\frac{5}{2}}}$$

$$\frac{2\zeta^3 \sqrt{x-\zeta}}{7(-1)}\Bigg|_0^x = -\frac{2}{7}\left[x^3\sqrt{0} - 0^3\sqrt{x}\right] = 0$$

$$\therefore \int_0^x \frac{\zeta^3}{\sqrt{x-\zeta}} d\zeta = \frac{6x}{7} \cdot \frac{16}{15} x^{\frac{5}{2}} = \frac{32}{35} x^{\frac{7}{2}}$$

By the same process, the fourth integral on the right hand side of Eq. (A-3) can be shown to be:

$$\int_0^x \frac{\zeta^4}{\sqrt{x-\zeta}} d\zeta = \frac{8x}{9} \frac{32}{35} x^{\frac{7}{2}} = \frac{256}{315} x^{\frac{9}{2}}$$

Upon substitution of integration results into Eqs. (A-3) and (A-2), we obtain:

$$\Rightarrow y(x) = \frac{1}{2\sqrt{x}} \frac{d}{dx}\left\{ a\frac{4}{3} x^{\frac{3}{2}} + b\frac{16}{15} x^{\frac{5}{2}} + c\frac{32}{35} x^{\frac{7}{2}} + d\frac{256}{315} x^{\frac{9}{2}} \right\}$$

$$y(x) = \frac{1}{2\sqrt{x}}\left\{ a\frac{4}{3}\frac{3}{2} x^{\frac{1}{2}} + b\frac{16}{15}\frac{5}{2} x^{\frac{3}{2}} + c\frac{32}{35}\frac{7}{2} x^{\frac{5}{2}} + d\frac{256}{315}\frac{9}{2} x^{\frac{7}{2}} \right\}$$

$$y(x) = \frac{1}{2}\frac{1}{x^{\frac{1}{2}}}\left\{ 2ax^{\frac{1}{2}} + \frac{8}{3} bx^{\frac{3}{2}} + \frac{16}{5} cx^{\frac{5}{2}} + \frac{128}{35} dx^{\frac{7}{2}} \right\}$$

Upon simplification,

$$\therefore y(x) = a + \frac{4}{3} bx + \frac{8}{5} cx^2 + \frac{64}{35} dx^3$$

Reverting back to our original notation, we have the following formula for intrinsic damping as a function of strain:

$$\therefore \eta(\varepsilon) = a + \frac{4}{3}b\varepsilon + \frac{8}{5}c\varepsilon^2 + \frac{64}{35}d\varepsilon^3 \tag{A-4}$$

where a, b, c, and d are the coefficients of the third-order polynomial which was used to fit the measured specimen damping.

Final note: for longitudinal specimen damping fit with an n-th order polynomial

$$\eta_s(\varepsilon_0) = \sum_{k=0}^{n} a_k \varepsilon_0^k$$

where a_0, a_1, a_2, $\ldots a_n$ are the coefficients of the n-th order polynomial, and ε_0 is the strain amplitude of the specimen, it can be shown (from recursion) that the following equation will result for intrinsic damping as a function of strain ε:

$$\eta(\varepsilon) = a_0 \frac{2^0 1!}{1}\varepsilon^0 + a_1 \frac{2^1 2!}{3\cdot 1}\varepsilon^1 + a_2 \frac{2^2 3!}{5\cdot 3\cdot 1}\varepsilon^2 + \cdots + a_n \frac{2^n (n+1)!}{(2n+1)\cdot(2n-1)\cdot(2n-3)\cdots 1}\varepsilon^n$$

This is a general form, which can be applied to longitudinal results requiring higher order polynomials to fit the specimen damping data.

APPENDIX B: DERIVATION OF RELATIONSHIP BETWEEN SPECIMEN DAMPING AND INTRINSIC DAMPING FOR A CANTILEVER BEAM

This derivation closely follows the process reported in reference [11]. Assume that the beam is slender and configured as shown in Figure B1. Therefore, we will neglect any effects which result from shear.

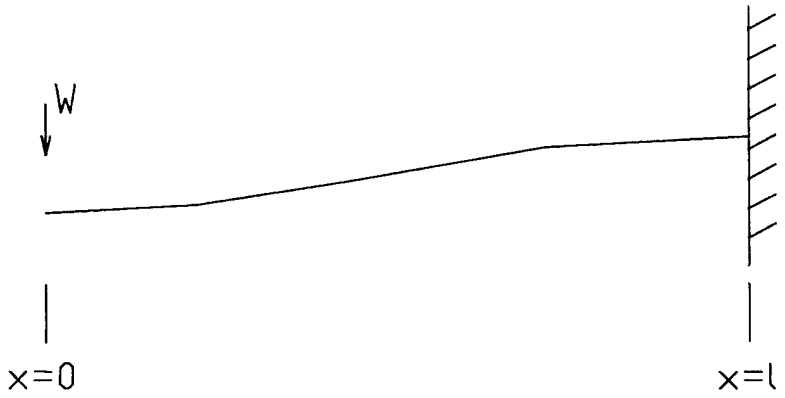

Figure B1. Schematic of cantilever beam.

The load W is applied at the origin of the coordinate system. The three dimensional sketch below indicates geometry and coordinate system. The axial stress and axial strain for the beam are as follows:

$$\sigma_{xx} = \frac{Wxy}{I}$$

$$\varepsilon_{xx} = \frac{\sigma_{xx}}{E} = \frac{W}{EI}xy$$

We need only examine the x-direction axial strain, shown in Figure B2, since Poisson induced strains do not contribute to strain energy in the sample:

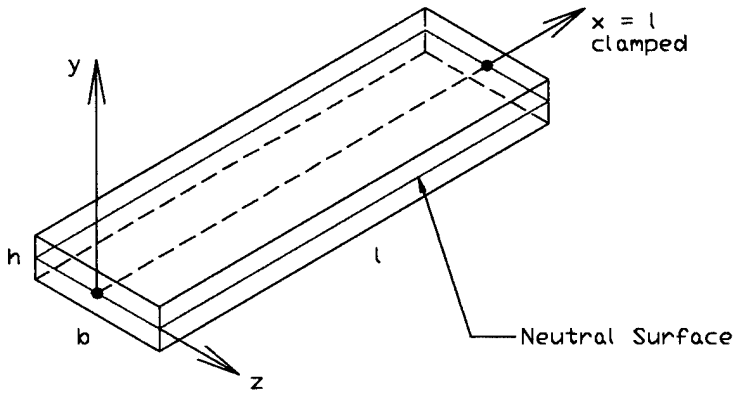

Figure B2. Sample coordinates

The energy dissipated per cycle in a specimen is as follows:

$$\Delta W_s V_s = \int_V \Delta W(\varepsilon) dV$$

where ΔW_s is the energy dissipated per unit volume, and V_s is the volume of the sample. Under the integral, ε represents strain, the infinitesimal volume increment is designated by dV, and $\Delta W(\varepsilon)$is the local energy dissipated per unit volume, which is strain dependent quantity. In the same manner as [11], we will employ the volume-strain function $dV/d\varepsilon$. Using the Lebnitz rule, we obtain:

$$\Delta W_s V_s = \int_0^{\varepsilon_s} \Delta W(\varepsilon) \frac{dV}{d\varepsilon} d\varepsilon$$

where ε_s is the maximum surface strain amplitude. The volume-strain function, $dV/d\varepsilon$, represents the region of volume where strains are less than or equal to a value ε. This function must first be determined before an attempt may be made to solve the integral.

Also, by definition:

$$\Delta W(\varepsilon) = 2\pi\eta(\varepsilon) W(\varepsilon)$$

where $\eta(\varepsilon)$ is the intrinsic damping loss factor, and $W(\varepsilon)$ is the strain energy per unit volume, defined as:

$$W(\varepsilon) = \frac{1}{2} \underbrace{M}_{\text{elastic modulus}} \varepsilon^2$$

The total energy dissipated by the specimen, per cycle, now becomes:

$$\Delta W_s V_s = \int_0^{\varepsilon_s} 2\pi\eta(\varepsilon) \frac{1}{2} M\varepsilon^2 \frac{dV}{d\varepsilon} d\varepsilon$$

$$\Delta W_s V_s = \frac{2\pi}{2} M \int_0^{\varepsilon_s} \varepsilon^2 \eta(\varepsilon) \frac{dV}{d\varepsilon} d\varepsilon$$

$$\therefore \Delta W_s = \frac{2\pi M}{2V_s} \int_0^{\varepsilon_s} \varepsilon^2 \eta(\varepsilon) \frac{dV}{d\varepsilon} d\varepsilon$$

Next, determine maximum strain energy stored per unit volume in the specimen

$$W_s V_s = \int_V W dV$$

$$W_s V_s = \int_0^{\varepsilon_s} \left(\frac{1}{2} M \varepsilon^2 \right) \frac{dV}{d\varepsilon} d\varepsilon$$

$$\therefore W_s = \frac{M}{2V_s} \int_0^{\varepsilon_s} \varepsilon^2 \frac{dV}{d\varepsilon} d\varepsilon$$

$$\therefore \eta(\varepsilon_s) = \frac{\Delta W_s}{2\pi W_s} = \frac{\int_0^{\varepsilon_s} \varepsilon^2 \eta(\varepsilon) \frac{dV}{d\varepsilon} d\varepsilon}{\int_0^{\varepsilon} \varepsilon^2 \frac{dV}{d\varepsilon} d\varepsilon} \qquad \text{(B-1)}$$

Before proceeding with integration, one must first determine the volume-strain function, $dV/d\varepsilon$, for the specific specimen design and loading. Two simple examples involving volume-strain function are given below. We will then proceed to the case of interest.

Example 1: Torsion of a cylindrical wire, outer radius r_s, length l. Strain amplitude is maximum (γ_s) at the specimen surface ($r = r_s$). The total volume (V_s) having strain less than or equal to γ_s is $\pi r_s^2 l$. The volume V having radius r with strain less than or equal to γ is $\pi r^2 l$

$$\gamma = \frac{r}{r_s} \gamma_s$$

$$\frac{V}{V_s} = \left(\frac{r}{r_s} \right)^2 = \left(\frac{\gamma}{\gamma_s} \right)^2$$

Therefore, the volume strain function is:

$$\frac{dV}{d\gamma} = 2 \frac{V_s}{\gamma_s^2} \gamma$$

We will now evaluate Eq. (B-1), except using shear strain γ in place of axial strain ε. The denominator of Eq. (B-1) is

$$\int_0^{\gamma_s} \gamma^2 \frac{dV}{d\gamma} d\gamma = 2 \frac{V_s}{\gamma_s^2} \int_0^{\gamma_s} \gamma^3 d\gamma = 2 \frac{V_s}{\gamma_s^2} \frac{\gamma_s^4}{4} \Bigg|_0^{\gamma_s} = \frac{1}{2} V_s \gamma_s^2$$

The numerator of Eq. (B-1) is

$$\int_0^{\gamma_s} \gamma^2 \eta(\gamma) \frac{dV}{d\gamma} d\gamma = 2 \frac{V_s}{\gamma_s^2} \int_0^{\gamma_s} \gamma^3 \eta(\gamma) d\gamma$$

Inserting the above results into Eq. (B-1), and re-arranging, produces the following result:

$$\frac{\gamma_s^4}{4}\eta_s(\gamma_s) = \int_0^{\gamma_s} \gamma^3 \eta(\gamma) d\gamma$$

Taking $d/d\gamma_s$ of both sides of the above equation produces:

$$\underbrace{\frac{d}{d\gamma_s}\left(\frac{\gamma_s^4}{4}\eta_s(\gamma_s)\right)}_{\frac{\gamma_s^4}{4}\frac{d\eta_s(\gamma_s)}{d\gamma_s}+\gamma_s^3\eta_s(\gamma_s)} = \underbrace{\frac{d}{d\gamma_s}\left(\int_0^{\gamma_s}\gamma^3\eta(\gamma)d\gamma\right)}_{\gamma_s^3\eta(\gamma_s)}$$

$$\Rightarrow \eta(\gamma_s) = \eta_s(\gamma_s) + \frac{\gamma_s}{4}\frac{d\eta_s(\gamma_s)}{d\gamma_s}$$

This is Eq. (4) in the main body of the report.

Example 2: Pure bending of a beam with rectangular cross-section. Use symmetry – consider only the upper half of the beam shown in Figure B3.

Width = b

Height = h

Length = l

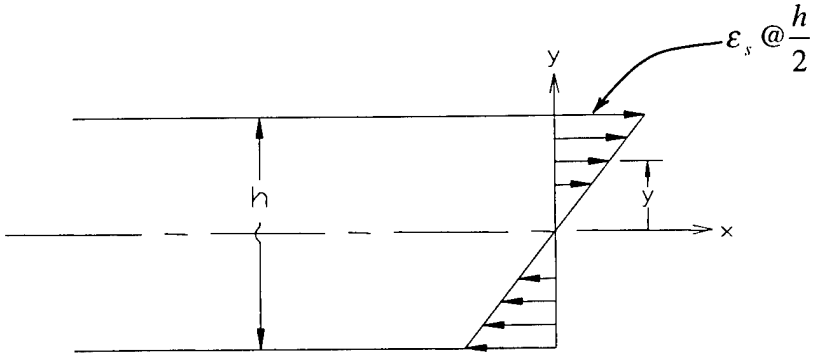

Figure B3. Schematic of pure bending of a beam with rectangular cross-section.

$$\varepsilon = \frac{y}{h/2}\varepsilon_s \qquad V = byl$$

$$= bly$$

$$\Downarrow \qquad \Downarrow$$

$$y = \frac{h/2}{\varepsilon_s}\varepsilon \qquad y = \frac{V}{bl}$$

$$\frac{h/2}{\varepsilon_s}\varepsilon = \frac{1}{bl}V$$

$$\Rightarrow V = \frac{blh}{2\varepsilon_s}\varepsilon$$

Considering V_s to be the volume of half the specimen (recall symmetry)

$$\frac{V}{V_s} = \frac{\varepsilon}{\varepsilon_s}$$

$$\therefore \frac{dV}{d\varepsilon} = \frac{V_s}{\varepsilon_s}$$

$$\int_0^{\varepsilon_s} \varepsilon^2 \frac{dV}{d\varepsilon} d\varepsilon = \frac{V_s}{\varepsilon_s}\int_0^{\varepsilon_s} \varepsilon^2 d\varepsilon$$

$$= \frac{V_s}{\varepsilon_s}\frac{\varepsilon^3}{3}\Bigg|_0^{\varepsilon_s} = \frac{1}{3}V_s\varepsilon_s^2$$

$$\int_0^{\varepsilon_s} \varepsilon^2\eta(\varepsilon)\frac{dV}{d\varepsilon} d\varepsilon = \frac{V_s}{\varepsilon_s}\int_0^{\varepsilon_s} \varepsilon^2\eta(\varepsilon) d\varepsilon$$

Substitution into Eq. (B-1) produces:

$$\eta_s(\varepsilon_s) = \frac{3}{\varepsilon_s^3}\int_0^{\varepsilon_s} \varepsilon^2\eta(\varepsilon) d\varepsilon$$

$$\Rightarrow \frac{\varepsilon_s^3\eta_s(\varepsilon_s)}{3} = \int_0^{\varepsilon_s} \varepsilon^2\eta\ (\varepsilon) d\varepsilon$$

Take $d/d\varepsilon_s$ of both sides of the above equation,

$$\underbrace{\frac{d}{d\varepsilon_s}\left(\frac{\varepsilon_s^3}{3}\eta(\varepsilon_s)\right)}_{\frac{\varepsilon_s^3}{3}\frac{d\eta_s(\varepsilon_s)}{d\varepsilon_s}+\varepsilon_s^2\eta_s(\varepsilon_s)} = \underbrace{\frac{d}{d\varepsilon_s}\left(\int_0^{\varepsilon_s}\varepsilon^2\eta(\varepsilon)d\varepsilon\right)}_{\varepsilon_s^2\eta(\varepsilon_s)}$$

$$\Rightarrow \eta(\varepsilon_s) = \frac{1}{\varepsilon_s^2}\left[\varepsilon_s^2\eta_s(\varepsilon_s) + \frac{\varepsilon_s^3}{3}\frac{d\eta_s(\varepsilon_s)}{d\varepsilon_s}\right]$$

$$\therefore \eta(\varepsilon_s) = \eta_s(\varepsilon_s) + \frac{\varepsilon_s}{3}\frac{d\eta(\varepsilon_s)}{d\varepsilon_s}$$

This is the result for a beam under pure bending. We now proceed to the case of the case of interest, the cantilever beam.

The problem of interest: Cantilever beam of rectangular section (length = l, width = b, height = h). The vibration shape of a cantilever in primary resonance is very similar to the shape of the beam when deflected in a quasi-static manner by a force on the tip of the beam. The strain field is for this shape depicted in Figure B4

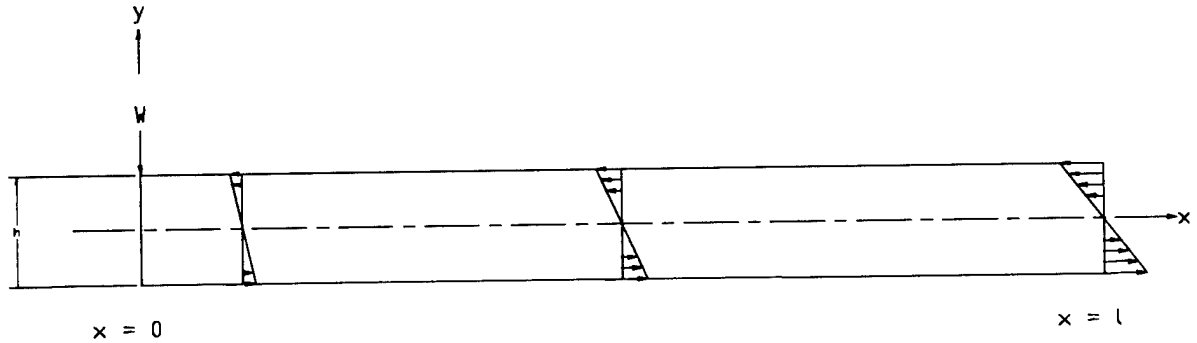

Figure B4. Vibrational shape of a cantilever in resonance.

Of course, when sub-resonant oscillations are present the same static bending shape is assumed. Using the results from static elasticity, we have:

Strain:

$$\varepsilon = \varepsilon_{xx} = \frac{W}{EI}xy$$

Therefore, the surface strain amplitude at any x, ε_{surf}, is:

$$\varepsilon_{surf} = \varepsilon(x, \tfrac{h}{2}) = \frac{Wh}{2EI}x$$

The maximum surface strain amplitude, ε_s, occurs at the root of the cantilever:

$$\varepsilon_s = \varepsilon_{surf}\Big|_{x=l} = \frac{Whl}{2EI}$$

$$\Rightarrow \frac{W}{EI} = \frac{2}{hl}\varepsilon_s$$

$$\therefore \varepsilon = \varepsilon_s \frac{xy}{l\,(h/2)}$$

or

$$\frac{\varepsilon}{\varepsilon_s} = \frac{xy}{l\,(h/2)} \quad \text{or} \quad \frac{h}{2}\frac{\varepsilon}{\varepsilon_s} = \frac{x}{l}y$$

A sketch of a line of constant ε is shown in Figure B5. The hatched area below the line of constant strain represents the region of volume where strain levels are less than ε. The line of constant strain falls off as $1/x$.

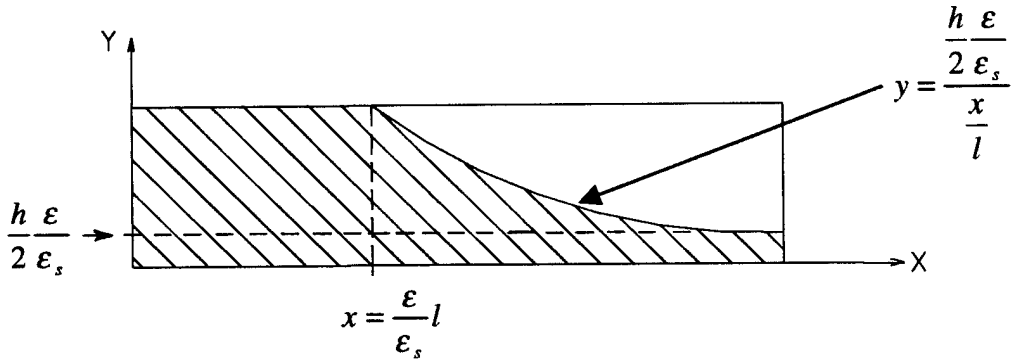

Figure B5. Plot of x-y space where $\varepsilon < \varepsilon_s$.

To get the volume-strain function, we need to calculate the volume V of the sample in which the axial strain is less than or equal to ε. Due to symmetry about the neutral axis, we need only consider only the top half of the beam.

$$V = b\left(\frac{\varepsilon}{\varepsilon_s} l\right)\left(\frac{h}{2}\right) + b\int_{\frac{\varepsilon}{\varepsilon_s} l}^{l}\int_{0}^{y} dy'dx$$

$$V = \frac{bhl}{2}\frac{\varepsilon}{\varepsilon_s} + b\underbrace{\int_{\frac{\varepsilon}{\varepsilon_s} l}^{l}\left(\frac{\frac{h}{2}\frac{\varepsilon}{\varepsilon_s}}{\frac{x}{l}}\right)dx}_{\frac{hl}{2}\frac{\varepsilon}{\varepsilon_s}\underbrace{\int_{\frac{\varepsilon}{\varepsilon_s} l}^{l}\frac{1}{x}dx}_{\ln x\Big|_{\frac{\varepsilon}{\varepsilon_s} l}^{l}}}$$

$$V = \frac{bhl}{2}\left[\frac{\varepsilon}{\varepsilon_s} + \ln l - \ln\frac{\varepsilon}{\varepsilon_s} l\right]$$

$$V = \frac{bhl}{2}\left[\frac{\varepsilon}{\varepsilon_s} + \ln l - \left(\ln\frac{\varepsilon}{\varepsilon_s} + \ln l\right)\right]$$

$$\therefore V = \frac{bhl}{2}\frac{\varepsilon}{\varepsilon_s}\left(1 - \ln\frac{\varepsilon}{\varepsilon_s}\right)$$

Upon continuing to consider only the upper half of the beam, we have:

$$V_s = \frac{bhl}{2}$$

$$\therefore \frac{V}{V_s} = \frac{\varepsilon}{\varepsilon_s}\left(1 - \ln\frac{\varepsilon}{\varepsilon_s}\right)$$

$$\text{or} \quad V = \frac{V_s}{\varepsilon_s}\left(1 - \ln\frac{\varepsilon}{\varepsilon_s}\right)\varepsilon$$

Now, taking a derivative with respect to strain produces the volume strain function.

$$\frac{dV}{d\varepsilon} = \frac{V_s}{\varepsilon_s} - \frac{V_s}{\varepsilon_s}\ln\frac{\varepsilon}{\varepsilon_s} - \underbrace{\frac{V_s}{\varepsilon_s}\varepsilon\frac{1}{\frac{\varepsilon}{\varepsilon_s}}\frac{1}{\varepsilon_s}}_{\frac{V_s}{\varepsilon_s}}$$

$$\therefore \frac{dV}{d\varepsilon} = -\frac{V_s}{\varepsilon_s}\ln\frac{\varepsilon}{\varepsilon_s}$$

We must next evaluate the numerator, N, and denominator, D, of the specimen loss factor equation, Eq. (B-1). This will allow us to determine the relationship between specimen loss factor and intrinsic loss factor.

$$\eta_s(\varepsilon_s) = \frac{N}{D} = \frac{\int_0^{\varepsilon_s} \varepsilon^2 \eta(\varepsilon)\frac{dV}{d\varepsilon}d\varepsilon}{\int_0^{\varepsilon_s} \varepsilon^2 \frac{dV}{d\varepsilon}d\varepsilon}$$

Evaluate denominator D first

$$D = \int_0^{\varepsilon_s} \varepsilon^2 \frac{dV}{d\varepsilon} d\varepsilon = -\frac{V_s}{\varepsilon_s} \underbrace{\int_0^{\varepsilon_s} \varepsilon^2 \ln\frac{\varepsilon}{\varepsilon_s} d\varepsilon}_{I_D}$$

$$I_D = \int_0^{\varepsilon_s} \varepsilon^2 (\ln\varepsilon - \ln\varepsilon_s) d\varepsilon$$

$$I_D = \underbrace{\int_0^{\varepsilon_s} \varepsilon^2 \ln\varepsilon d\varepsilon}_{\underbrace{\int_0^{\varepsilon_s} \ln\varepsilon \left(\frac{\varepsilon^3}{3}\right)}_{\underbrace{\left(\frac{\varepsilon^3}{3}\ln\varepsilon\right)\Big|_0^{\varepsilon_s} - \int_0^{\varepsilon_s} \frac{\varepsilon^3}{3}\frac{1}{\varepsilon} d\varepsilon}_{\frac{\varepsilon_s^3}{3}\ln\varepsilon_s - \frac{1}{3}\underbrace{\int_0^{\varepsilon_s} \varepsilon^2 d\varepsilon}_{\underbrace{\frac{1}{3}\left(\frac{\varepsilon^3}{3}\right)\Big|_0^{\varepsilon_s}}_{\frac{1}{9}\varepsilon_s^3}}}}} - \ln\varepsilon_s \underbrace{\int_0^{\varepsilon_s} \varepsilon^2 d\varepsilon}_{\underbrace{\frac{\varepsilon^3}{3}\Big|_0^{\varepsilon_s}}_{\frac{\varepsilon_s^3}{3}\ln\varepsilon_s}}$$

$$\Rightarrow I_D = \frac{\varepsilon_s^3}{3}\ln\varepsilon_s - \frac{1}{9}\varepsilon_s^3 - \frac{\varepsilon_s^3}{3}\ln\varepsilon_s$$

$$I_D = -\frac{1}{9}\varepsilon_s^3$$

$$\therefore D = \frac{1}{9}\frac{V_s}{\varepsilon_s}\varepsilon_s^3$$

Next, evaluate the numerator N

$$N = \int_0^{\varepsilon_s} \varepsilon^2 \eta(\varepsilon) \frac{dV}{d\varepsilon} d\varepsilon$$

$$= \int_0^{\varepsilon_s} \varepsilon^2 \eta(\varepsilon) \left(-\frac{V_s}{\varepsilon_s}\ln\frac{\varepsilon}{\varepsilon_s}\right) d\varepsilon$$

$$N = -\frac{V_s}{\varepsilon_s}\int_0^{\varepsilon_s} \varepsilon^2 \ln\frac{\varepsilon}{\varepsilon_s}\eta(\varepsilon) d\varepsilon$$

$$N = -\frac{V_s}{\varepsilon_s}\left[\int_0^{\varepsilon_s} \varepsilon^2 \ln\varepsilon\,\eta(\varepsilon) d\varepsilon - \ln\varepsilon_s \int_0^{\varepsilon_s} \varepsilon^2 \eta(\varepsilon) d\varepsilon\right]$$

Forming the ratio *N/D*, the result for specimen loss factor becomes:

$$\eta_s(\varepsilon_s) = -\frac{9}{\varepsilon_s^3}\left[\int_0^{\varepsilon_s} \varepsilon^2 \ln\varepsilon\,\eta(\varepsilon)d\varepsilon - \ln\varepsilon_s \int_0^{\varepsilon_s} \varepsilon^2\eta(\varepsilon)d\varepsilon\right]$$

or

$$-\frac{\varepsilon_s^3}{9}\eta_s(\varepsilon_s) = \int_0^{\varepsilon_s} \varepsilon^2 \ln\varepsilon\,\eta(\varepsilon)d\varepsilon - \ln\varepsilon_s \int_0^{\varepsilon_s} \varepsilon^2\eta(\varepsilon)d\varepsilon$$

Taking $d/d\varepsilon_s$ of both sides of the above equation, the left hand side (LHS) and right hand side (RHS) become:

$$\text{LHS} = \frac{d}{d\varepsilon_s}\left(-\frac{\varepsilon_s^3}{9}\eta(\varepsilon_s)\right) = -\frac{\varepsilon_s^3}{9}\frac{d\eta_s(\varepsilon_s)}{d\varepsilon_s} - \frac{\varepsilon_s^2}{3}\eta_s(\varepsilon_s)$$

$$\text{RHS} = \frac{d}{d\varepsilon_s}\left(\int_0^{\varepsilon_s} \varepsilon^2 \ln\varepsilon\,\eta(\varepsilon)d\varepsilon - \ln\varepsilon_s \int_0^{\varepsilon_s} \varepsilon^2\eta(\varepsilon)d\varepsilon\right)$$

The RHS consists of two terms, which are evaluated separately, below:

(1r)
$$\frac{d}{d\varepsilon_s}\int_0^{\varepsilon_s} \varepsilon^2 \ln\varepsilon\eta(\varepsilon)d\varepsilon = \varepsilon_s^2 \ln\varepsilon_s\eta(\varepsilon_s)$$

(2r)
$$\frac{d}{d\varepsilon_s}\left(\ln\varepsilon_s\int_0^{\varepsilon_s} \varepsilon^2\eta(\varepsilon)d\varepsilon\right) = \ln\varepsilon_s\left(\varepsilon_s^2\eta(\varepsilon_s)\right) + \frac{1}{\varepsilon_s}\int_0^{\varepsilon_s} \varepsilon^2\eta(\varepsilon)d\varepsilon$$

$$\therefore RHS = \varepsilon_s^2 \ln\varepsilon_s\eta(\varepsilon_s) - \ln\varepsilon_s\left(\varepsilon_s^2\eta(\varepsilon_s)\right) - \frac{1}{\varepsilon_s}\int_0^{\varepsilon_s} \varepsilon^2\eta(\varepsilon)d\varepsilon$$

$$\therefore \frac{\varepsilon_s^3}{9}\frac{d\eta_s(\varepsilon_s)}{d\varepsilon_s} + \frac{\varepsilon_s^2}{3}\eta_s(\varepsilon_s) = \frac{1}{\varepsilon_s}\int_0^{\varepsilon_2} \varepsilon^2\eta(\varepsilon)d\varepsilon$$

OR

$$\frac{\varepsilon_s^4}{9}\frac{d\eta_s(\varepsilon_s)}{d\varepsilon} + \frac{\varepsilon_s^3}{3}\eta_s(\varepsilon_s) = \int_0^{\varepsilon_s} \varepsilon^2\eta(\varepsilon)d\varepsilon$$

Again, take $d/d\varepsilon_s$ of both sides of the above equation. On first examining the first and second terms of the LHS, we have:

(1l) $$\frac{d}{d\varepsilon_s}\left(\frac{\varepsilon_s^4}{9}\frac{d\eta(\varepsilon_s)}{d\varepsilon_s}\right)=\frac{\varepsilon_s^4}{9}\frac{d^2\eta_s(\varepsilon_s)}{d\varepsilon^2{}_s}+\frac{4}{9}\varepsilon_s^3\frac{d\eta_s(\varepsilon_s)}{d\varepsilon_s}$$

(2l) $$\frac{d}{d\varepsilon_s}\left(\frac{\varepsilon_s^3}{3}\eta(\varepsilon_s)\right)=\frac{\varepsilon_s^3}{3}\frac{d\eta_s(\varepsilon_s)}{d\varepsilon_s}+\varepsilon_s^2\eta_s(\varepsilon_s)$$

Next, evaluating the RHS, we have:

$$\frac{d}{d\varepsilon_s}\left(\int_0^{\varepsilon_s}\varepsilon^2\eta(\varepsilon)d\varepsilon\right)=\varepsilon_s^2\eta(\varepsilon_s)$$

Therefore, we arrive at the following result, which is the desired relationship between specimen damping and intrinsic damping for a material with nonlinear damping characteristics.

$$\frac{\varepsilon_s^4}{9}\frac{d^2\eta_s(\varepsilon_s)}{d\varepsilon_s^2}+\frac{7}{9}\varepsilon_s^3\frac{d\eta_s(\varepsilon_s)}{d\varepsilon_s}+\varepsilon_s^2\eta_s(\varepsilon_s)=\varepsilon_s^2\eta(\varepsilon_s)$$

$$\therefore\eta(\varepsilon_s)=\eta_s(\varepsilon_s)+\frac{7}{9}\varepsilon_s\frac{d\eta_s(\varepsilon_s)}{d\varepsilon_s}+\frac{1}{9}\varepsilon_s^2\frac{d^2\eta_s(\varepsilon_s)}{d\varepsilon_s^2}$$

This is Eq. (5) in the main body of the report.

APPENDIX C: DERIVATION OF RELATIONSHIP BETWEEN SPECIMEN DAMPING AND INTRINSIC DAMPING FOR A FIXED-GUIDED BEAM

A diagram showing the loading of fixed-guided beam is shown in Figure C1. R_A and R_B represent the reaction forces developed at ends A and B, respectively. θ_A and θ_B represent the angular rotations at ends A and B, respectively. M_A and M_B represent the reaction moments developed at ends A and B, respectively. Y is deflection.

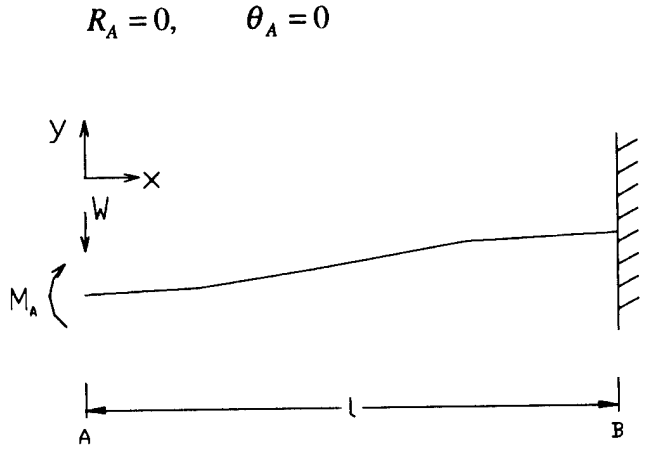

Figure C1. Loading of a fixed-guided beam.

As a matter of convention let the x coordinate be collinear with the centroidal axis of the beam. Therefore, y is the distance from the centroid of the undeformed beam. The end deflection of the fixed-guided beam is:

$$Y_A = -\frac{Wl^3}{12EI} \quad \text{End Deflection}$$

where I is the second moment of area of the beam cross-section, about the z axis. Deflection, rotation, moment, and shear values elsewhere along the length of the beam may be calculated using the following equations:

$$\text{Deflection:} \quad Y = Y_A + \theta_A x + \frac{M_A x^2}{2EI} + \frac{R_A x^3}{6EI} - \frac{Wx^3}{6EI}$$

$$\text{Rotation:} \quad \theta = \theta_A + \frac{M_A x}{EI} + \frac{R_A x^2}{2EI} - \frac{Wx^2}{2EI}$$

$$\text{Moment:} \quad M = M_A + R_A x - Wx$$

$$\text{Shear:} \quad V = R_A - W$$

Inserting zeros for R_A and θ_A, the equations become:

$$\text{Shear:} \quad V = -W$$

$$\text{Moment:} \quad M = M_A - W_X$$

$$\text{Rotation:} \quad \theta = \frac{M_A x}{EI} - \frac{Wx^2}{2EI}$$

$$\text{Deflection:} \quad Y = Y_A + \frac{M_A x^2}{2EI} - \frac{Wx^3}{6EI}$$

Plugging in known values for M_A and y_A, the above results simplify to the following:

$$V = -W$$

$$M = \frac{Wl}{2} - Wx$$

$$\theta = \frac{Wlx}{2EI} - \frac{Wx^2}{2EI}$$

$$Y = -\frac{Wl^3}{12EI} + \frac{Wlx^2}{4EI} - \frac{Wx^3}{6EI}$$

The conditions of stress within a section of the beam are given next.

$$\text{Fiber Stress:} \quad \sigma_{xx} = -\frac{My}{I} = -\frac{W}{I}\left(\frac{l}{2} - x\right)y$$

$$\text{Shear Stress:} \quad \overline{\sigma}_{yx} = \overline{\sigma}_{xy} = \frac{V}{Ib}\int_A y dA = \frac{V}{2I}\left(\left(\frac{h}{2}\right)^2 - y^2\right)$$

Now, for convenience, let us do a coordinate transformation to make the "built-in" end of the beam occur at x=0. We will keep y in the same direction (up). This will make the top surface of the beam, at the root of the clamp, the position of maximum strain amplitude, with positive strain and stress for the loading shown. Note also that there is 4-quadrant symmetry in this problem.

Let $X = l - x$ (or $x = l - X$))

When $x = 0,\ X = l$
$x = l,\ X = 0$

Also let $Z = -z$

[The z coordinate transform makes no difference, since there is no z dependence in the problem. But by setting $z = -z$, the new coordinate system is right-handed.]

Shear: $V = -W$

Moment: $M = \frac{Wl}{2} - W(l - X) = WX - \frac{Wl}{2}$

Rotation: $\theta = \frac{W}{2EI}(l - x)x = \frac{W}{2EI}X(l - X) = \frac{Wl}{2EI}X - \frac{W}{2EI}X^2$

Deflection: $Y = -\frac{Wl^3}{12EI} + \frac{W}{2EI}\left(\frac{lx^2}{2} - \frac{x^3}{3}\right) = -\frac{Wl^3}{12EI} + \frac{W}{2EI}\left(\frac{l}{2}(l - X)^2 - \frac{1}{3}(l - X)^3\right)$

The main quantities that we need are as shown in Figure C2.

$V = -W$ and $M = WX - \frac{Wl}{2}$

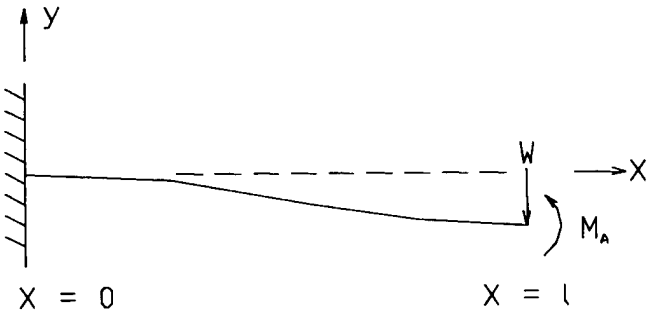

Figure C2. Loading on centroid of beam.

Now, revert notation back to the use of the lower case x and z for the new coordinate system. That is, simply let $x = X$ and $z = Z$. The geometry and loading is shown in Figure C3.

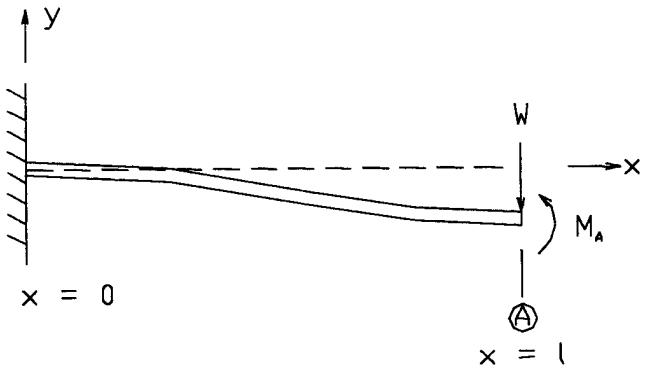

Figure C3. Loading on fixed-guided beam with changed coordinates.

Section Loads:

$$V = -W$$

$$M = W\left(x - \frac{l}{2}\right)$$

Section Stresses:

$$\sigma_{xx} = -\frac{My}{I}$$

$$\sigma_{xx} = -\frac{1}{I}W\left(x - \frac{l}{2}\right)y$$

$$\overline{\sigma}_{xy} = \frac{V}{2I}\left(\left(\frac{h}{2}\right)^2 - y^2\right) = -\frac{W}{2I}\left(\left(\frac{h}{2}\right)^2 - y^2\right)$$

Simplify Problem: neglect shear stresses by assuming that they are at least an order of magnitude smaller than the fiber stresses. This requires that we assume a long slender beam.

Also, note the symmetry properties shown in Figure C4.

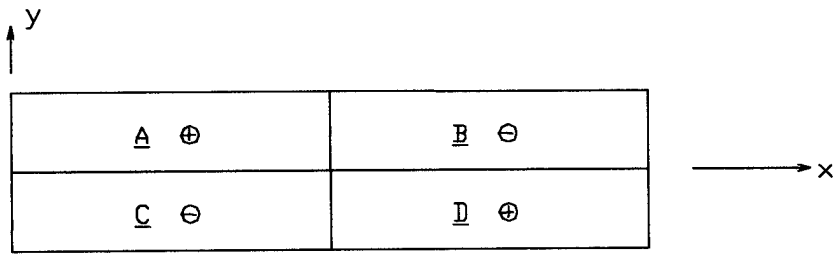

Figure C4. Symmetry of system.

The stresses and strain fields in A and D are equal at points of symmetry. The symmetry is mirror-like about the center of the beam: stresses on the upper surface at the root are identical

to those on the lower surface at the top. The stresses and strains in A and D are positive while those in B and C are negative.

So in computations for volume strain function, we need only consider quadrant A, or, the region in x-y space bounded by $0 \le y \le h/2$, $0 \le x \le l/2$.

For this simplified problem

$$\varepsilon_{xx} = \frac{\sigma_{xx}}{E} = -\frac{W}{EI}\left(x - \frac{l}{2}\right)y$$

Simply refer to ε_{xx} as ε

$$\therefore \varepsilon = \frac{W}{EI}\left(\frac{l}{2} - x\right)y$$

The maximum strain amplitude, ε_s, occurs at the upper surface at the root ($y=h/2$, $x=0$).

$$\therefore \varepsilon_s = \frac{Whl}{4EI}$$

Rewrite the expression for ε to include ε_s

$$\varepsilon = \frac{W\frac{h}{2}\frac{l}{2}}{EI}\left(1 - \frac{x}{l/2}\right)\frac{y}{h/2}$$

$$\varepsilon = \frac{Whl}{4EI}\left(1 - \frac{x}{l/2}\right)\frac{y}{h/2}$$

$$\therefore \varepsilon = \varepsilon_s\left(1 - \frac{x}{l/2}\right)\frac{y}{h/2}$$

Determination of Volume-Strain Function: define locus of points in x-y space where ε is constant, and where $\varepsilon < \varepsilon_s$. This is shown in Figure C5.

$$\frac{h}{2}\frac{\varepsilon}{\varepsilon_s} = \left(1 - \frac{x}{l/2}\right)y$$

$$\therefore y = \frac{\frac{h}{2}\frac{\varepsilon}{\varepsilon_s}}{1 - \frac{x}{l/2}}$$

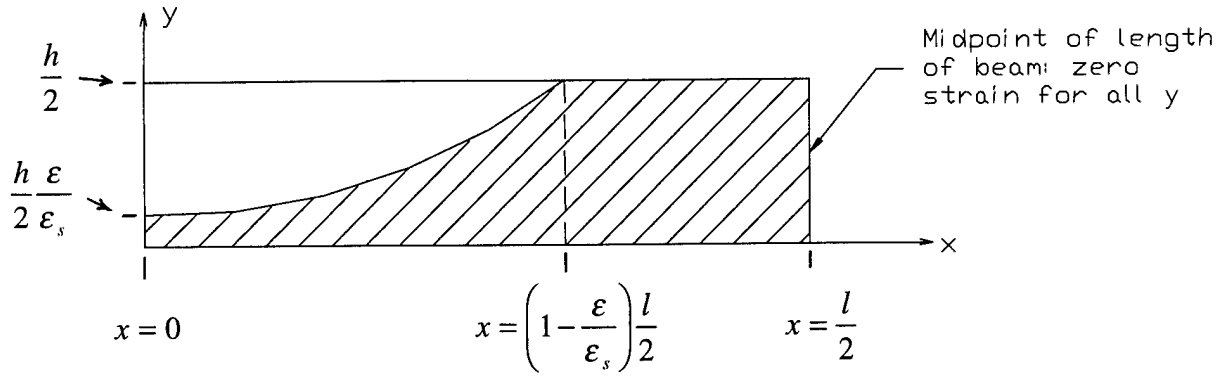

Figure C5. Locus of points where ε is constant and less than ε_s.

Determine the volume of the sample (or, in this case the quarter sample) where the strain is less than or equal to ε.

$$dV = bdydx$$

$$V = b \int_{\substack{Cross- \\ Hatched \\ Area}} dydx$$

$$V = b\underbrace{\int_0^{\left(1-\frac{\varepsilon}{\varepsilon_s}\right)\frac{l}{2}} \int_0^{y} dydx}_{I} + \underbrace{b\left[\frac{l}{2} - \left(1-\frac{\varepsilon}{\varepsilon_s}\right)\frac{l}{2}\right]\frac{h}{2}}_{\frac{bhl}{4}\left(\frac{\varepsilon}{\varepsilon_s}\right)}$$

$$I = \int_0^{\left(1-\frac{\varepsilon}{\varepsilon_s}\right)\frac{l}{2}} \int_0^{y} dydx = \int_0^{\left(1-\frac{\varepsilon}{\varepsilon_s}\right)\frac{l}{2}} \frac{(h/2)(\varepsilon/\varepsilon_s)}{1-\frac{x}{l/2}} dx = \frac{h}{2}\frac{\varepsilon}{\varepsilon_s} \int_0^{\left(1-\frac{\varepsilon}{\varepsilon_s}\right)\frac{l}{2}} \frac{dx}{1-\frac{x}{l/2}}$$

Let $\gamma = 1 - \frac{x}{l/2} \quad \Leftrightarrow \quad \gamma - 1 = -\frac{x}{l/2}$

$$x = \frac{l}{2}(1-\gamma) \qquad dx = -\frac{l}{2}d\gamma$$

when $x = 0 \qquad \gamma = 1$

$$x = \left(1-\frac{\varepsilon}{\varepsilon_s}\right)\frac{l}{2} \qquad \gamma = \frac{\varepsilon}{\varepsilon_s}$$

$$\Rightarrow I = \frac{h}{2}\frac{\varepsilon}{\varepsilon_s}\left(-\frac{l}{2}\right)\int_1^{\frac{\varepsilon}{\varepsilon_s}} \frac{d\gamma}{\gamma} = \frac{hl}{4}\frac{\varepsilon}{\varepsilon_s}\ln\gamma\Big|_1^{\frac{\varepsilon}{\varepsilon_s}} = -\frac{hl}{4}\frac{\varepsilon}{\varepsilon_s}\left[\ln\frac{\varepsilon}{\varepsilon_s} - \ln 1\right]$$

$$\therefore V = \frac{bhl}{4}\left[\frac{\varepsilon}{\varepsilon_s} - \frac{\varepsilon}{\varepsilon_s}\ln\left(\frac{\varepsilon}{\varepsilon_s}\right)\right]$$

$$\text{or } V = \frac{bhl}{4}\frac{\varepsilon}{\varepsilon_s}\left[1 - \ln\left(\frac{\varepsilon}{\varepsilon_s}\right)\right]$$

Note: For the section of the specimen under study (quarter sample):

$$V_s = \frac{bhl}{4}$$

$$\therefore V = \frac{V}{\varepsilon_s}\varepsilon\left(1 - \ln\left(\frac{\varepsilon}{\varepsilon_s}\right)\right)$$

or

$$\frac{V}{V_s} = \frac{\varepsilon}{\varepsilon_s}\left(1 - \ln\left(\frac{\varepsilon}{\varepsilon_s}\right)\right)$$

or, perhaps more conveniently

$$V = \frac{V_s}{\varepsilon_s}\left(1 - \ln\frac{\varepsilon}{\varepsilon_s}\right)\varepsilon$$

$$\text{so,} \quad \frac{dV}{d\varepsilon} = -\frac{V_s}{\varepsilon_s}\ln\frac{\varepsilon}{\varepsilon_s}$$

This is the same volume-strain function as was derived for the case of a regular cantilever beam. Therefore, the process required to finish the derivation is exactly the same as that which was done for the cantilever beam (with tip load only), as in the Appendix B. The relationship between specimen damping and intrinsic damping is as follows:

$$\therefore \eta(\varepsilon_s) = \eta_s(\varepsilon_s) + \frac{7}{9}\varepsilon_s\frac{d\eta_s(\varepsilon_s)}{d\varepsilon_s} + \frac{1}{9}\varepsilon_s^2\frac{d^2\eta_s(\varepsilon_s)}{d\varepsilon_s^2}$$

Initial Distribution

Copies	
2	Commander Office of Naval Research 800 N. Quincy St Arlington VA 22217
1	Code 332 (Kabacoff)
1	Code 332 (Sedricks)
2	DTIC
1	Dr Vikram Kinra Texas A&M university Aerospace Engineering Dept College Station, TX 77843-3141
1	Dr. Enrique Lavernia University of California at Irvine Materials Science and Engineering Irvine, CA 92717-2700
1	Ahid Nashif Roush Anatrol 10895 Indeco Dr Cincinnati, OH 45241
1	David Van Aken University of Missouri Rolla Department of Mechanical Engineering Rolla, MO 65401-0249
1	Manfred Wuttig University of Maryland Materials and Nuclear Engineering Dept College Park, MD 20742-2115

Copies	Center Distribution
27	Commander Naval Surface Warfare Center Carderock Division Bethesda MD 20084-5000
1	Code 61
1	Code 612
1	Code 612 (Wong)
1	Code 84
1	Code 842
20	Code 842 (Graesser)
1	Code 3443 (TIC/S)
1	Code 3442 (TIC/C)
1	Prof. Andre Riviere Laboratoire De Mechanique Et Physique Des Materiaux ENSMA Rue Guillanme VII 86034 Poitiers Cedex FRANCE
1	Kari Ullakko Helsinki University of Technology Laboratory of Engineering Materials Puumiehenkuja 3A SF-02150 Espo FINLAND
1	Jan Van Humbeeck NFWO MTM-K.U.Leuven De Croylaan 2 B-3001 Heverlee BELGIUM